Australian Government
Department of Defence
Defence Science and
Technology Group

Elasto–Plastic 3D Finite Element Contact Analysis of a Hole Containing a Circular Insert in a Fatigue Test Coupon

Witold Waldman

Aerospace Division
Defence Science and Technology Group

DST-Group-TR-3140

ABSTRACT

Aircraft structures typically contain large numbers of circular holes that are fitted with fasteners such as bolts or rivets. During the service life of aircraft, fatigue damage often occurs at such holes. The analysis of the stress distributions occurring around the boundaries of holes in the presence of fasteners is therefore of importance in fatigue life studies, particularly at higher load levels where the effects of material plastic deformation become significant. This report is primarily concerned with the results of a three-dimensional elasto–plastic finite element contact analysis of a typical aluminium fatigue test coupon containing a hole that is fitted with a zero-clearance titanium fastener. The response to separate tension and compression loading was considered. The peak levels of stress concentration and their locations in the presence of varying amounts of material plasticity were determined. The elasto–plastic study was augmented by a 3D linear-elastic investigation of the stress concentration behaviour when the hole is fitted with low-tolerance fasteners that have varying levels of clearance. The linear-elastic and elasto–plastic results presented here are relevant for use in test interpretation and validation activities in relation to the full-scale fatigue test of the BAE Systems Lead-In Fighter Hawk jet trainer aircraft in service with the Royal Australian Air Force.

RELEASE LIMITATION

Approved for public release

Published by

Aerospace Division
Defence Science and Technology Group
506 Lorimer Street
Fishermans Bend, Victoria 3207, Australia

Telephone: 1300 333 362
Fax: (03) 9626 7999

AR-016-369
August 2015

APPROVED FOR PUBLIC RELEASE

Elasto–Plastic 3D Finite Element Contact Analysis of a Hole Containing a Circular Insert in a Fatigue Test Coupon

Executive Summary

Aerospace Division has been deeply involved in the development and application of technologies that help to ensure the safety and enhance the availability of aircraft in service with the Royal Australian Air Force by extending the fatigue lives of airframe structural components. Many of these aircraft structures typically contain large numbers of circular holes that are fitted with fasteners. Fatigue damage often occurs at such holes during the service life of the aircraft, with attendant increases in operating costs and maintenance times. The analysis of stress distributions that occur around the boundaries of holes in the presence of fasteners is therefore of significant importance in fatigue life studies, many of which involve extensive and costly experimental fatigue testing of representative coupons undergoing programmed constant-amplitude or spectrum loading.

Some linear-elastic two-dimensional plane elasticity solutions are available for the contact stresses caused by a circular disk inserted into a circular hole in an infinite plate undergoing remote uniaxial loading. One of the known available solutions is applicable to the commonly-occurring case where the plate material and the insert material have different elastic properties. Within its limitations, the exact analytical/numerical solution for this class of problem can be used to assist in the validation of other general-purpose computational approaches that can be applied to solving three-dimensional contact problems, such as finite element analysis. However, there is no available three-dimensional elasto–plastic contact solution for the stress distribution occurring at holes in plates fitted with unloaded fasteners.

In this report, the advanced contact analysis capability of the Abaqus finite element analysis code has been used to determine the nonlinear three-dimensional elasto–plastic contact stress distributions around a circular hole in an aluminium plate that is fitted with an unloaded titanium insert. In the linear-elastic behaviour regime, the Abaqus results have been validated using a known two-dimensional analytical/numerical solution technique, thus providing some measure of confidence in the results of the elasto–plastic analyses. It has been determined that the elasto–plastic material deformation that occurs at the fastener hole, both with and without an insert fitted, serves to significantly reduce the stress concentration factor at the hole. This behaviour will affect the fatigue lives of the coupons during testing, and therefore needs to be taken into consideration during subsequent fatigue test interpretation and validation activities. The results presented here are relevant to the test interpretation and validation activities related to the full-scale fatigue test of the BAE Systems Lead-In Fighter Hawk jet trainer aircraft in service with the Royal Australian Air Force.

Author

Witold Waldman
Aerospace Division

Mr Witold Waldman completed a BEng (with distinction) in Aeronautical Engineering at the Royal Melbourne Institute of Technology in 1981. He commenced work in Structures Division in 1982 at what was then the Aeronautical Research Laboratory. He has published a number of papers and reports, and his experience has focussed on stress analysis using finite element and boundary element methods, structural mechanics, fracture mechanics, computational unsteady aerodynamics, structural dynamics testing, digital filtering of flight test data, nonlinear optimisation, and spectral analysis. His recent work has been in the areas of structural shape optimisation and computation of stress intensity factors. He is currently a Senior Research Engineer in the Structural and Damage Mechanics Group in the Airframe Technology and Safety Branch of Aerospace Division within the Defence Science and Technology Group, Department of Defence.

Contents

Nomenclature

A_p	area of plastic zone
a	radius of hole
d	diameter of circular hole in plate
d_p	depth of plastic zone
e	engineering strain
E	Young's modulus
E_i	Young's modulus of insert material
E_p	Young's modulus of plate material
H	height of plate
K_t	stress concentration factor
P	load level
R	load ratio under cyclic loading
r	radius of hole in plate
s	engineering stress
S	remote stress
S_{rr}	radial stress
S_{tt}	tangential stress
S_x	remote stress aligned with x-direction
S_y	remote stress aligned with y-direction
S_{yc}	remote compression stress aligned with y-direction
S_{yt}	remote tension stress aligned with y-direction
t	thickness of plate
W	width of plate
x	rectangular Cartesian x-coordinate
y	rectangular Cartesian y-coordinate
z	rectangular Cartesian z-coordinate
θ	polar angle
ε	true strain
ε_p	plastic strain
ε_{pl}	true strain at proportional limit
ε_{cpl}	true strain at cyclic proportional limit
η_t	contact angle between plate and insert for plate loaded in tension
η_c	contact angle between plate and insert for plate loaded in compression
υ	Poisson's ratio
υ_i	Poisson's ratio of insert material
υ_p	Poisson's ratio of plate material
Ψ	ratio of the K_t of the filled hole to the K_t of the empty hole
σ	true stress
σ_1 σ_2 σ_3	principal stresses
σ_{pl}	true stress at proportional limit
σ_{cpl}	true stress at cyclic proportional limit
σ_{rr}	radial stress
σ_{tt}	tangential stress
σ_{vm}	von Mises stress
σ_{xx} σ_{yy} σ_{zz}	direct stresses
τ_{xy} τ_{yz} τ_{zx}	shear stresses

1. Introduction

Aerospace Division of the Defence Science and Technology Group regularly designs and uses metallic fatigue testing coupons to aid in the fatigue life and structural integrity management of Royal Australian Air Force (RAAF) airframes. An aluminium-alloy fatigue test coupon (see Figure 1) has been designed and applied in support of the validation of test interpretation activities associated with the BAE Systems Lead-In Fighter (LIF) Hawk full-scale fatigue test that has been undertaken by BAE Systems for the RAAF. This coupon is known as the LIF Hawk Filled Hole Coupon and is intended to be utilised in fatigue crack initiation and crack growth studies. It incorporates a centrally-located circular hole, and low-clearance titanium fasteners are inserted into the hole during testing. These low-clearance fasteners approximate the neat-fit fastener case, which corresponds to the situation where the diametric clearance between the interior bore of the hole and the cylindrical outer surface of the fastener is zero.

It is well known that stress concentration levels at fastener holes are very high, and can lead to fatigue failures in service. It is also well known that cold working the surface of the hole or using interference-fit fasteners reduces the stress concentration effect at the fastener hole, by developing a field of beneficial residual stresses around the wall of the hole. Prior workers have performed two-dimensional (2D) and three-dimensional (3D) elasto–plastic finite element analysis (FEA) of such holes [1–5], sometimes including fatigue life analysis studies. Their work has demonstrated the benefit of using cold working or fitting either interference-fit or neat-fit fasteners in comparison with empty non-cold-worked holes. In even earlier work involving the elasto–plastic analysis of a uniaxially-loaded thin narrow strip of a strain-hardening material perforated with a circular hole [6], it was noted that the level of stress concentration decreases continuously from its linear-elastic value as the plastic zone evolves.

In the past, some workers have used boundary element analysis techniques to analyse 2D elasto–plastic hole–pin contact problems [7, 8], including analyses of unloaded rigid pins fitted in uniaxially-loaded elasto–plastic plates. Although similar to the present problem of interest, the use of a rigid pin, as well as the 2D nature of the solutions, places a significant limitation on their applicability to the present fatigue test coupon. These 2D solutions inherently do not account for any through-thickness effects that can only be included in a 3D analysis. It is noted here that a search of the literature did not find any reported work on the subject of 3D elasto–plastic analysis of loaded plates with holes fitted with unloaded pins.

The test interpretation activities associated with the LIF Hawk full-scale fatigue test require a detailed and accurate knowledge of the stress concentration factor, K_t, that typically occurs at holes. At sufficiently high levels of loading, holes fitted with neat-fit fasteners will experience the effects of plasticity, and this will affect the peak K_t. In order to gain useful insights about such behaviours, the LIF Hawk Filled Hole Coupon was analysed using 3D finite element contact analysis with a view to providing the following solutions:

a. Linear-elastic analysis of the K_t versus tension-load response using hole–pin combinations with various diametric clearances, ranging in value from 0 mm to 0.01 mm.

b. Elasto–plastic analysis of the K_t versus load response under tension and compression loading for the case of a neat-fit pin inserted into the hole.

c. Quantification of the elasto–plastic stress decay at the minimum cross-section.

The Abaqus FEA code was previously successfully utilised in an extensive 2D and 3D investigation into the linear-elastic contact behaviour of the LIF Hawk Filled Hole Coupon with the hole containing a neat-fit titanium circular insert [9]. The analysis used available 2D analytical/numerical contact stress solutions for a uniaxially-loaded [10] and a biaxially-loaded [11] infinite plate with a smooth circular disc insert, both of which assumed that no shear continuity exists at the plate–insert interface. The Wilson [11] solution includes the effects of the plate and the insert being made from materials with different elastic moduli, which allowed the contact stresses arising from the interaction of the aluminium coupon and the titanium fastener to be computed.

When a non-interference-fit fastener is inserted into the hole in the coupon, the greatest reduction in K_t is obtained for the case of a neat-fit insert. Hence, as the neat-fit case is a limit condition, the present 3D elasto–plastic FEA using the Abaqus code focusses on this particular case. Analysis of the neat-fit case provides a bound for the maximum reduction in K_t that can be expected, in conjunction with a similar bound provided by analysis of the coupon with an empty hole. The neat-fit case is an example of a conforming contact problem, as the boundary of the hole and the surface of the insert touch at multiple points before any deformation occurs.

Details of the geometry of the LIF Hawk Filled Hole Coupon are provided in Section 2. The general elasto–plastic input data requirements for the Abaqus FEA code are explained in Section 3. Section 4 gives the nominal elastic and elasto–plastic material properties of the coupon, as well as those of the pin that is used to model the presence of the fastener in the hole. The results of a 3D linear-elastic finite element contact analysis of the hole–pin configuration for a range of hole–pin clearance gaps are presented in Section 5. The general approach that was utilised in performing the elasto–plastic contact analyses using Abaqus is presented in Section 6. The results of 3D elasto–plastic FEA studies for a neat-fit titanium pin fitted into the hole in the aluminium coupon are given in Section 7. The conclusions derived from the present work are presented in Section 8, and some suggestions for potential follow-on work are included.

2. Coupon geometry and loading configuration

The general geometry and dimensions of the LIF Hawk Filled Hole Coupon are shown in Figure 1. The coupon shape takes on the common “dog-bone” configuration, in this instance with a narrowing at the centre section corresponding to a 2:1 taper in width in the transverse x-direction. The coupon is loaded uniaxially in the longitudinal y-direction. The thickness of the coupon is t = 6 mm, and a circular hole of nominal diameter d = 6.35 mm is located in the centre of each coupon. The coupon is manufactured from aerospace aluminium alloy material (see Section 4 for further details). Unloaded close-fit fasteners of small diametric clearance were fitted in the hole during the coupon fatigue testing program. The fasteners

are manufactured from a titanium alloy commonly used in aerospace applications (see Section 4 for further details).

The geometrically idealised configuration of a plate with a hole, with the plate loaded by a uniaxial tensile stress S_{yt} at infinity, showing the contact angle η_t between the plate and the unloaded circular disk insert is depicted in Figure 2. The angular position around the hole boundary is measured from the x-axis and is denoted by θ, which is positive in the anti-clockwise direction. The Young's modulus and Poisson's ratio for the plate are denoted by E_p and υ_p, and for the insert by E_i and υ_i. In a similar manner, Figure 3 depicts the geometrical configuration of a hole in a plate that is loaded by a uniaxial compressive stress S_{yc} at infinity showing the contact angle η_c between the plate and the circular disk insert.

For the plate loaded in uniaxial tension, the contact zone is symmetrical about the x-axis. The left and right regions of the hole contract in a direction perpendicular to the direction of the applied loading, with a gapping condition developing at the top and bottom of the hole (see Figure 2).

For the plate loaded in uniaxial compression, the situation is reversed, with the contact zone now being symmetrical about the y-axis. The top and bottom regions of the hole contract in a longitudinal direction in line with the direction of the applied loading, with a gapping condition developing along the left and right sides of the hole (see Figure 3).

3. Abaqus elasto–plastic input data requirements

The aluminium and titanium alloys used in the coupon and fastener material display linear-elastic behaviour at low strain magnitudes, each with their own constant value of elastic modulus. At high levels of stress and strain, these materials begin to have a nonlinear behaviour that includes an inelastic response, which is called plasticity. The shift from elastic to plastic behaviour occurs at what is called the *yield point* or the *proportional limit*. The strain and the attendant stress at the proportional limit are denoted by ε_{pl} and σ_{pl}. Below the yield point, the deformation of the metal is purely elastic, and the elastic strains are fully recovered upon removal of the load. When the stress in the metal exceeds the yield stress, plastic (permanent) deformation begins to occur, resulting in plastic strains. Deformation of the metal in the post-yield region results in the accumulation of both elastic and plastic strains. Once the material yields, the post-yield deformation region is characterised by a significant reduction in material stiffness compared to the elastic modulus. An important feature of metal plasticity is that the plastic deformation is associated with nearly incompressible material behaviour (no change in material volume), which restricts the choice of elements that can be used in elasto–plastic finite element simulations of structural stress–strain response.

The Abaqus FEA program has a number of different options that can be used to simulate the inelastic behaviour of metals. Nonlinear problems are solved by applying the loading in steps, with any given step being divided into a number of load increments. The equations that represent the response of the structure to the applied loading are solved iteratively at each load increment. When any material point in the structure yields, its stress components are updated for that load increment. The elasto–plastic material response formulation that is

used in Abaqus is based on a curve of *true stress* versus *true strain*. However, it is the engineering strain e (length change per unit undeformed length) and engineering stress s (force per unit undeformed area) material properties that are usually measured under uniaxial tension and/or compression coupon tests. In such circumstances, it is necessary to be able to convert the measured elasto–plastic material data from engineering (nominal) stress–strain values to true stress–strain values. The following relationships are valid only prior to the onset of necking in the uniaxial material test specimen.

The relation between the true strain ε and engineering strain e is given by the following equation:

$$\varepsilon = \ln(1+e) \tag{1}$$

The relation for true stress σ in terms of engineering stress s is simply:

$$\sigma = (1+e)s \tag{2}$$

From the above equations, it is evident that the true stress and the true strain will be within 2% of their nominal stress–strain equivalents for small values of nominal strain $e \leq 0.02$.

It is a requirement of the metal plasticity model used in Abaqus that the post-yield behaviour be defined in terms of the true stress σ and the true plastic strain ε_p. The following equation can be used to convert true strain to true plastic strain:

$$\varepsilon_p = \varepsilon - \frac{\sigma}{E} \tag{3}$$

It is also necessary to ensure that the modulus of elasticity, E, corresponds to the slope defined by the yield point at the proportional limit of the material on the true stress–strain curve, (ε_{pl}, σ_{pl}). The value of E can be computed from the following relation:

$$E = \frac{\sigma_{pl}}{\varepsilon_{pl}} \tag{4}$$

Fatigue damage involves a process of crack initiation and growth that is caused by the application of a cyclic loading. Hence, when performing fatigue life calculations of notched components, of which the present coupon is one such example, it is necessary to consider the cyclic material behaviour. For many metallic aerospace materials, the stress–strain response under cyclic loading is different than that which occurs under the application of a single monotonic load. Some degree of cyclic strain softening occurs at low strain amplitudes and results in a lower cyclic stress response.

The cyclic stress–strain curve is a geometric construct that is defined by the locus of reversal points of the series of stable hysteresis loops (see Figure 4). These stable loops are generated by fully-reversed ($R = -1$) strain cycling over a range of strain amplitudes that involve cyclic deformation in the plastic regime. Like the monotonic stress–strain curve, the cyclic stress–strain curve has a linear region where the strains are elastic, and a nonlinear region where

the strains are plastic. The stress at the upper limit of the linear region is referred to as the cyclic proportional limit, σ_{cpl}, with a corresponding strain of ε_{cpl}. The proportional limit can be estimated from inspection of the cyclic stress–strain curve. The overall curve is assumed to be symmetric about the origin, whereby the stress–strain relationship is the same in compression as it is in tension.

Abaqus approximates the smooth true plastic stress–strain behaviour of a metallic material with a series of straight line segments joining the set of user-supplied data points. As it is possible to use any number of data points, by using a large number of them it is then possible to create a very good approximation of the actual behaviour. The first data point that is provided defines the initial yield stress of the material, σ_{pl}, and by definition it has a plastic strain value of $\varepsilon_p = 0$. Abaqus performs linear interpolation between the provided data points in order to compute the stress–strain response of the material. It also assumes that the stress response remains constant when the maximum provided plastic strain value is exceeded.

4. Material properties

For the purpose of the analyses in this report, the coupon material properties are chosen to be representative of 7050-T74 aluminium alloy. The fastener material is taken to be Ti-6AL-4V titanium alloy. These two materials are assumed to exhibit isotropic, elastic behaviour up to each of their respective proportional limits. The 7050-T74 alloy displays a value of σ_{cpl} that is lower than that for many other aluminium alloys, hence it will display greater amounts of plastic deformation. This will serve to provide a useful limiting case that highlights the maximum expected K_t-reducing effects of plasticity around the boundary of the hole. The upper bound corresponds to the fully-elastic case that was previously analysed in [9]. As a simple initial approximation, using the K_t of 3.0 determined from the linear-elastic hole–pin contact analysis in [9], plastic deformation for 7050-T74 will begin to occur at a tension load of approximately P = 16 kN (47% of the maximum load applied during the coupon testing program). Note that it is purely coincidental that the peak K_t of 3.0 used here corresponds to the well-known theoretical K_t of an empty circular hole in a 2D infinite plate remotely loaded in uniaxial tension.

4.1 Coupon material data

Cyclic stress–strain curve data corresponding to aluminium alloy 7050-T74 material was obtained in terms of a small set of engineering stress–strain data points. These were converted to true stress–strain values using the relations provided earlier. The resultant cyclic true stress–strain curve is shown in Figure 5, and the data points are given in Table 1. As specified in the data, the yield stress at the cyclic proportional limit is σ_{cpl} = 276.89 MPa, with a corresponding yield strain of ε_{cpl} = 0.003992 mm/mm. Using these two values, the elastic modulus of the aluminium alloy was computed to be E_p = 69.362 GPa. Using available data published in [12], the Poisson's ratio was taken to be υ_p = 0.33, which is representative of aluminium alloys in general.

4.2 Fastener material data

For the titanium alloy Ti-6AL-4V fastener (insert) material, the cyclic true stress–strain curve is shown in Figure 6, and the set of data points is given in Table 2. The yield stress at the cyclic proportional limit was estimated from this curve to be σ_{cpl} = 410.24 MPa, with a corresponding yield strain of ε_{cpl} = 0.00375 mm/mm. The elastic modulus was computed to be E_i = 109.397 GPa, and from available data published in [12] the Poisson's ratio was taken as being equal to υ_i = 0.31.

4.3 Interpolated plastic true stress–strain material data

In order to provide a high-fidelity representation of the true plastic stress–strain response for use with Abaqus, cubic spline interpolation was performed on the available 7050-T74 and Ti-6Al-4V material data. In both cases, a greater density of points was created in the region just following the onset of plastic deformation, as this area exhibited the greatest nonlinear behaviour. Table 3 gives the 77 interpolated values of the plastic stress–strain data pairs that were obtained for the aluminium alloy 7050-T74. Similarly, Table 4 gives the 93 interpolated values of the plastic stress–strain data pairs that were obtained for the titanium alloy Ti-6Al-4V (STA) L. These values were used to create the appropriate elasto–plastic material models in Abaqus for use in the analyses.

5. Linear-elastic 3D finite element contact analysis results

5.1 Geometry and meshing

Abaqus 6.9-1 was used for the analyses reported in this section, and Abaqus/CAE 6.9-1 was used as the pre- and post-processor. For the purposes of creating the 3D geometry in Abaqus, an orthogonal *x*-*y*-*z* coordinate system was defined with its origin at the geometric centre of the dog-bone coupon (see Figure 1). The horizontal *x*-axis is aligned parallel to the transverse direction of the coupon, the vertical *y*-axis is aligned parallel to the longitudinal direction of the coupon, and the *z*-axis is aligned parallel to the thickness direction of the coupon. To help reduce the model size, and hence lower computation times, ⅛ symmetry was used when creating the finite element mesh. This also had the side benefit of opening up various interior surfaces of the structure where it was anticipated that the peak stresses would be developed, making the job of stress visualisation somewhat more straightforward.

Figure 7 shows the Abaqus finite element mesh that was created for conducting the linear-elastic analysis of the plate and pin combination. The lower picture shows the general mesh of the entire ⅛-symmetry model, and the upper picture shows a detail of the mesh in the immediate vicinity of the hole. The pin is nominally modelled as a hand-tightened loose-fit bolt in a hole, without any of the restraints that normally would apply to a bolt head and nut combination in a fully torqued-up bolt. In the FEA model, the pin extends 1 mm beyond each of the outer longitudinal faces of the plate. To some degree, this is anticipated to simulate the presence of the additional material that is associated with the bolt at the head and nut ends.

The mesh used for the coupon and the pin was predominantly composed of 20-noded quadratic C3D20 hexahedral brick elements. Some 15-noded quadratic C3D15 elements were

also present. In developing the mesh, the coupon was partitioned into subregions, and use was made of structured as well as automated swept meshing. A total of 6592 elements were defined using 23266 nodes. There were 61386 degrees of freedom present in the model.

5.2 Applied loading

Loads were applied in the longitudinal direction as a uniform pressure acting over the faces of the solid elements located along the bottom of the coupon mesh. The 0–35 kN load range was divided into 28 load increments, with each load increment being 1.25 kN in size. For the maximum tension load of P = 35 kN, the remote uniform tensile stress applied to the ends of the coupon was 97.22 MPa. With the chosen degree of mesh refinement and total number of load increments, the time taken to obtain a solution ranged from about 1½ minutes for the empty-hole case to 16 minutes for a hole–pin gap size of 0 mm (where contact occurs immediately).

5.3 Contact analysis considerations

This is a mixed boundary condition problem with moving boundaries, where the surfaces of the pin and the hole in the plate can come into contact with each other. The stiffness of the assembly will change when the initial hole–pin gap closes and contact is made between the pin and the plate. Therefore, nonlinear analysis with an incremental application of loading is required in order to model the transition from the non-contacting state to the contacting state. The broad assumptions used for this nonlinear analysis are:

- Material: linear-elastic, isotropic, homogenous.
- Zero friction.
- Small sliding.
- In-plane remote uniaxial tension loading applied to ends of the plate (maximum 35 kN load).
- No pin loading.
- No compression loading.
- The initial hole–pin gap is uniform.
- Both the pin and the hole can deform during contact.
- Advancing contact behaviour (contact area increases with load).

The frictionless surface-to-surface contact model available in Abaqus was used for analysing the hole–pin contact behaviour. The Abaqus default parameter settings were used. The Abaqus documentation recommends that the master contact surface consist of the more rigid and/or more highly refined surface. Hence, as the mesh densities used on the pin and the hole were quite similar, the master surface was defined to be the pin, which is made from titanium and is about 65% stiffer than the aluminium material from which the coupon is manufactured. The slave contact surface was defined to be the surface of the hole.

A small number of linear-elastic FEA solutions were determined for various fastener clearance levels deemed to be representative of those encountered during fatigue testing. In this report, the term “gap” refers to half the initial clearance level, which corresponds to the distance from the pin to the edge of the hole when the pin is located centrally in the hole. The

gap sizes that have been considered are: 0 mm (neat-fit), 0.0005 mm, 0.0010 mm, 0.0020 mm, 0.0025 mm, 0.0030 mm, 0.0040 mm, 0.0050 mm, and 0.0100 mm.

5.4 Results for the empty-hole case

A linear-elastic 3D analysis of the empty-hole coupon for this level of mesh refinement was conducted using the Abaqus FEA code. The stress concentration factor based on the gross cross-section of the coupon at the hole was determined to be $K_t = 3.347$ at $(x, y, z) = (-3.175, 0, 0)$. It is instructive to compare this 3D result to those obtained by other workers analysing similar 2D and 3D geometries.

From the data presented in Chart 4.1 of *Peterson's Stress Concentration Factors* [13] for a 2D finite-width thin plate with a circular hole, an expression for K_t in terms of plate width W and hole diameter d is given as:

$$K_t = 0.284 + 2/(1 - d/W) - 0.600(1 - d/W) + 1.32(1 - d/W)^2 \quad (5)$$

For the present coupon geometry, $W = 30$ mm and $d = 6.35$ mm, giving $d/W = 0.2117$ and $K_t = 3.168$. Note that the equation for K_t as printed in [13] contains a typographical error, and the corrected version of the equation in question is given above. (The publisher was notified of this error and has issued an erratum.) Using this K_t value, the 2D finite-width correction (FWC) factor is computed to be $3.168/3 = 1.056$.

Folias and Wang [14] have determined a 3D through-thickness K_t solution for a circular hole in an infinite plate of arbitrary thickness. They obtained a peak value of $K_t = 3.181$ for a plate with $d/t = 1$ for $\upsilon = 0.33$. For the present coupon, $d/t = 1.0583$, and so by interpolating the results provided by Folias and Wang we obtain $K_t = 3.175$. If we apply the 2D FWC factor to this interpolated result, we obtain $K_t = 3.353$, which is just 0.2% greater than the value obtained from the 3D FEA. The results obtained by Folias and Wang for a plate with $\upsilon = 0.33$ and $d/t = 1$, with the previously-computed 2D FWC factor of 1.056 applied to them, are plotted in Figure 8. Also shown there are the 3D FEA results for the empty-hole coupon. It is evident that the two sets of results are in very good agreement.

An elastic analysis of pin joints has previously been presented by Rao [15]. From the theoretical formulation given therein, the following expression for the transverse displacement u_{edge} of the edge of a circular hole of radius R_{hole} in an infinitely-large thin plate that is uniaxially loaded by a stress σ can be derived as being equal to:

$$u_{\text{edge}} = R_{\text{hole}}\sigma/E \quad (6)$$

For a uniaxial remote tensile load of 35 kN applied to the coupon, which corresponds to a gross-section (without the hole) average tensile stress of $\sigma = 194.4$ MPa in the central region of the coupon, the predicted inward displacement of the hole edge is $u_{\text{edge}} = 0.00895$ mm.

The following equations for u_r and u_θ give the 2D plane stress displacement field around a circular hole in an infinitely-large thin plate undergoing uniform tensile remote loading.

$$u_r = \frac{\sigma r}{2E}\cos(2\theta)\left((1+\nu)+4\frac{a^2}{r^2}-(1+\nu)\frac{a^4}{r^4}\right)+\frac{\sigma r}{2E}\left((1-\nu)+(1+\nu)\frac{a^2}{r^2}\right)$$
$$u_\theta = -\frac{\sigma r}{2E}\sin(2\theta)\left((1+\nu)+2(1-\nu)\frac{a^2}{r^2}+(1+\nu)\frac{a^4}{r^4}\right) \quad (7)$$

In the above equations, a is the radius of the hole, (r, θ) are the polar coordinates of a point in the plate measured relative to the centre of the hole, and θ is measured positive in the anticlockwise direction away from the vertical axis. Hence, the equation for u_{edge} is obtained simply by substituting $r = a$ and $\theta = 90°$ into the expression for u_r.

As obtained from the 3D FEA, Figure 9 shows the through-thickness variation of the horizontal displacement, u_x, of the side of the empty hole where the horizontal plane of symmetry intersects the hole. The coupon is loaded in uniaxial tension with an average gross-section stress (without the hole) corresponding to σ at the centre of the coupon. For generality, the displacement u_x is presented in nondimensional form as $u_x/(R_{hole}\sigma/E)$, where R_{hole} is the radius of the hole in the coupon. It is apparent that the displacement u_x is not entirely uniform through the thickness, being 12.7% greater at the outside surface of the plate than at the midplane. For a remote loading of 35 kN, under linear-elastic conditions, the u_x displacement at the midplane of the empty hole is 0.00969 mm, while at the outside surface it is 0.01092 mm.

The above analysis indicates that, for the present hole diameter of 6.35 mm and 35 kN load level, gaps larger than about 0.011 mm will not produce any contact at all. Without any contact between the hole and pin, there will, of course, be no propping of the hole and therefore no reduction in K_t.

The analytical formula for the edge displacement can be modified to include a simple finite-width correction based on the average of the gross-section and net-section stresses. This leads to the following estimate for u_{edge}:

$$u_{edge} = 0.5\left[1+W/(W-d)\right]R_{hole}\sigma/E \quad (8)$$

For the present geometry, we therefore have that $u_{edge} = 1.134R_{hole}\sigma/E$, which places the displacement approximately midway between the upper and lower bounds of the 3D displacement profile that was computed using 3D FEA.

5.5 Results for the filled-hole case

5.5.1 Tangential stress distribution around the hole

A plot of the angular distribution of normalised tangential stress, S_{tt}/S_{yt}, around the hole edge at the midplane of the plate is shown in Figure 10 for a tension load level of 35 kN and initial gap sizes of 0 mm, 0.0025 mm and 0.0050 mm, and also for the empty-hole case. As the hole–pin gap increases in size, the peak tangential stress gets progressively higher, and the peak value and the stress distribution itself approach the results obtained for the empty-hole case. The wiggles in the tangential stress response in the vicinity of $\theta = 60°$, where $S_{tt}/S_{yt} \approx 0$,

occur as a result of the relatively coarse nature of the finite element mesh that was used, and are not of any concern; they will disappear with a small degree of mesh refinement.

For the Gap = 0.0050 mm case, contact between the hole and the pin has resulted in a peak in the curve located at $\theta = \eta_t = 11.8°$. Symmetry conditions imply that the peak is present at four locations around the hole boundary, corresponding to $\theta = \pm 11.8°$ and $\theta = \pm 168.2°$. For the Gap = 0.0025 mm case, the peak occurs at $\theta = 15.8°$. For the Gap = 0 mm (neat-fit) case, the peak occurs at $\theta = 20.1°$. Of course, for the empty-hole case the peak is located at $\theta = 0°$. It appears that, as the size of the gap increases, the angular location of the peak in K_t moves closer to the empty-hole result. Furthermore, the 3D FEA analysis reported in [9] showed that the angular location of the peak increases significantly when going from the midplane to the free surface due to 3D effects; for the present coupon, this increase amounts to about 3.5° for the Gap = 0 mm case.

For the analysis of the Gap = 0.0050 mm case, the overclosure that is evident in the Abaqus contact solution is 0.0001 mm at the centre of the contact interface between the hole and pin. Overclosure is the amount by which the slave surface (the hole boundary) extends into the master surface (the pin) at the constraint locations over the contact boundary. The 0.0001 mm overclosure amounts to 2% of the initial gap size of 0.005 mm, and is of the order of 0.05% of the nominal element size in that region. The low value of overclosure is an indicator that an accurate solution has been achieved, within the limits of the chosen level of mesh refinement.

5.5.2 Radial stress distribution around the hole

A plot of the angular distribution of normalised radial stress, S_{rr}/S_{yt}, around the hole edge at the midplane of the plate is shown in Figure 11 for a tension load level of 35 kN and initial hole–pin gap sizes of 0 mm, 0.0025 mm and 0.0050 mm. The radial stress caused by contact between the pin and the hole is compressive in nature.

For each of the gap cases, the peak stress occurs at the $\theta = 0°$ location. The maximum response in the radial stress occurs for the neat-fit hole–pin condition, corresponding to Gap = 0 mm. As the hole–pin gap increases in size, the peak radial stress gets progressively lower. The peak value of radial stress for the Gap = 0 mm case is $S_{rr}/S_{yt} = 0.770$, while for the Gap = 0.0050 mm case it is $S_{rr}/S_{yt} = 0.513$, which is a reduction of 33%.

The extent of the contact arc is represented by the region where the radial stress is non-zero in magnitude. From prior work [9, 10, 11], the presence of a relatively sharp transition to a zero value of radial stress at the edge of the contact zone was expected. However, due to the coarseness of the mesh, this transition region is more rounded in the current analysis. Additional mesh refinement would enable the stresses in this region of rapid stress transition to be determined with greater accuracy, as indicated by the results of the mesh refinement studies that were previously reported in [9].

5.5.3 Maximum principal stress distribution

A stress contour plot of the maximum principal stress field for the empty-hole case and a 35 kN load is shown in Figure 12, while Figure 13 shows the results obtained for an initial gap size of 0.0025 mm at the same load level. Figure 14 shows a series of stress contour plots

for the 0.0025 mm gap case, with each plot normalised to the peak value of the maximum principal stress. This series of plots depicts how the stress field changes as the load is increased in 5 kN increments from 5 kN to 35 kN. Note that the point of maximum stress progressively moves its way around the hole from θ = 0° at 5 kN load to about θ = 15.8° at 35 kN load. Contour plot (h), which is the last plot in the lower right-hand corner, is for the empty-hole case at 35 kN. The distribution of stress relative to the peak maximum principal stress at each load level in contour plots (a) to (c) is the same as that shown in (h), which indicates that hole–pin contact did not occur in cases (a) through (c).

Note that the number of stress contour levels and their colours in Abaqus/CAE was configured to be the same as that typically used by MSC Patran when plotting results as stress contours. For ease of future reference, the RGB colour coordinates of each of the ten colours that were used are given in Table 5.

5.5.4 Stress concentration load response for family of hole–pin gaps

A set of maximum K_t versus load plots for a range of gaps and also the empty-hole case is presented in Figure 15. Here the value of K_t was based on the peak value of the maximum principal stress occurring along the arc of hole boundary at the midplane of the coupon. The gap sizes range in value from 0.0 mm to 0.010 mm. As expected, the empty-hole case is the one that results in the highest stress concentration factor. The minimum value of K_t = 2.717, which is 18.8% lower than for the empty-hole case, is achieved for the Gap = 0.0 mm case, and the stress concentration factor is constant across the full load range that has been considered. For the Gap = 0.0050 mm case, K_t starts off at the empty-hole value of 3.347, and begins to reduce slowly when the load level exceeds 17.5 kN, reaching a low of K_t = 2.886 when the load reaches 35 kN. At this point, K_t is only 13.8% lower than for the empty-hole case. The analysis also indicates that incipient contact for the Gap = 0.0100 mm case, corresponding to a hole–pin diametric clearance of 0.02 mm, occurs at the maximum load of 35 kN. As a result, gaps greater than this will not produce any contact at all and therefore there will be no reduction effect on K_t.

The variation of K_t with load at the θ = 0° midplane location corresponding to the point defined by the coordinates (x, y, z) = (–3.175, 0, 0), is shown in Figure 16. This point lies on the hole at the point of minimum cross-section. The response at this location shows a wider band of variation of K_t versus load for all gap sizes, varying from 3.347 down to 2.717. This is not unexpected, as the peak value of K_t will often occur elsewhere around the arc of the hole, as was shown previously in Figure 15.

5.5.5 Stress decay at minimum cross-section

The variation of K_t versus the normalised distance from the hole centre, x/R_{hole}, for an initial gap size of 0.005 mm and remote loads of 20 kN and 35 kN, as well as the empty-hole case (which is load independent), is shown in Figure 17 for $1.0 \le x/R_{\text{hole}} \le 2.0$. At a distance equal to one hole radius away from the hole edge, the stress has already decayed to within approximately 28% of the gross-section average stress (represented by K_t = 1.0). For the 35 kN case, when $x/R_{hole} < 1.3$, the stresses are in the plastic range for the aluminium material, and are thus not truly accurate as represented here, although the general shape of

the K_t decay curve is expected to be similar. The K_t decay curves over a reduced range $1.0 \leq x/R_{hole} \leq 1.2$ and for two different gap sizes, 0.0025 mm and 0.0050 mm, are shown in Figure 18. This more clearly shows the differences between the various K_t decay responses.

6. Elasto-plastic 3D finite element analysis approach

6.1 General assumptions and considerations

The problem under consideration is a mixed boundary condition problem with moving boundaries, where the surfaces of the pin (fastener) and the hole in the plate come into contact with each other. The broad assumptions used for this nonlinear elasto–plastic analysis are:

- Material: elasto–plastic, isotropic, homogenous.
- Zero friction (no shear continuity on the hole–pin interface).
- Small sliding.
- The initial hole–pin gap is zero (neat-fit fastener).
- Both the pin and the hole can deform during contact.
- No pin loading.
- In-plane remote uniaxial loading applied to ends of the plate (maximum 35 kN tension load, or maximum 14 kN compression load).

A hole–pin gap of zero has been chosen for the elasto–plastic investigation as the linear-elastic analysis indicated that the neat-fit case produces the greatest reduction in peak stress around the hole boundary. The fact that the initial hole–pin gap is zero means that this is a conformal contact problem, where the hole and the pin are assumed to touch at multiple points before any deformation of either of them takes place. In the absence of friction, the contact arc will fully develop to its linear-elastic steady-state value as soon as any load is applied to the plate. In the linear-elastic material response regime, the resulting stress distributions will be in direct proportion to the applied load, but the extent of the contact arc will remain constant. Once the linear-elastic limits of the plate or the pin material are exceeded, an incremental application of the loading is required in order to model what has now become elasto–plastic contact behaviour.

6.2 Geometry and meshing

Abaqus/Standard 6.11-1 was used for the elasto–plastic analyses, and Abaqus/CAE 6.11-1 was used as the pre- and post-processor. For the purposes of creating the 3D geometry in Abaqus, the same orthogonal x-y-z coordinate system as was used for the linear-elastic analysis case was defined here, with its origin at the geometric centre of the dog-bone coupon (see Figure 1). As before, ⅛-symmetry boundary conditions were used when creating the finite element mesh in order to reduce the size of the model.

Figure 19 shows the Abaqus finite element mesh that was created for analysing the plate and pin combinations, including the location of the origin of the x-y-z coordinate system. A graded mesh was developed for this model based on the results presented in [9], providing a compromise between computational accuracy and execution time. The upper left picture shows the general mesh of the entire ⅛-symmetry model. The upper right picture provides a

side-on view of the plate and pin mesh showing the grading of the mesh spacing around the hole–pin boundary.

The bottom picture in Figure 19 shows the mesh in the immediate vicinity of the hole–pin interface. Due to the presence of a singularity in the radial stress along the hole boundary at the interface where the free outer surface of the coupon meets the pin, the mesh in that vicinity has been refined. By refining the mesh in this manner, it is hoped to be able to better capture the high radial stresses that are occurring in that location, and in this way more accurately simulate the elasto–plastic flow during development of the plastic zone with increasing load levels. The existence of the stress singularity near the edges of contact regions is quite well known (see, for example, Conway *et al*. [16]), and is covered in greater detail in the analysis presented in [9] with regard to the specific geometry of the LIF Hawk Filled Hole Coupon.

The pin is nominally modelled as a hand-tightened neat-fit bolt in a hole, without any of the restraints that normally would apply to a bolt head and nut combination in a fully torqued-up bolt. In the finite element model, the pin extends 1 mm beyond each of the outer longitudinal faces of the plate. To some degree, this is anticipated to simulate the presence of the additional material that is associated with the bolt at the head and nut ends.

The finite element mesh was predominantly composed of 20-noded quadratic C3D20 hexahedral brick elements. Some 15-noded quadratic C3D15 elements were also present. In developing the mesh, the coupon and the pin were partitioned into subregions, and use was made of structured meshing as well as automated swept meshing. The coupon mesh consisted of 22882 elements, and the pin mesh consisted of 7784 elements. There were approximately 440,000 degrees of freedom present in the model.

6.3 Applied loading

Loads were applied as a uniform pressure over the faces of the solid elements located along the bottom of the coupon mesh. For the tension loading, the 0–35 kN load range was applied as a linear ramp divided into 20 load increments, with each load increment being 1.75 kN in size. For the maximum tension load of P = 35 kN, the remote uniform tensile stress applied to the ends of the coupon was 97.22 MPa. For the compression loading, the 0–14 kN load range was applied as a linear ramp divided into 10 load increments, with each load increment being 1.4 kN in size. For the maximum compression load of P = 14 kN, the remote uniform compressive stress applied to the ends of the coupon was 38.89 MPa.

6.4 Contact parameters

The frictionless surface-to-surface contact model available in Abaqus was used for analysing the hole–pin contact behaviour. Apart from specifying that displacement-based parabolic extrapolation be utilised in place of linear extrapolation from one load increment to the next, the default Abaqus parameter settings were used. The Abaqus documentation recommends that the master contact surface consist of the more rigid and/or more highly refined surface. Hence, as the mesh densities used on the pin and the hole were quite similar, the master

surface was defined to be the titanium pin. The surface of the hole was then defined to be the slave contact surface.

6.5 Plasticity parameters

Abaqus has available a number of different models of plasticity behaviour. For the present analysis, the *isotropic hardening model* was chosen to represent the post-yield behaviour. In this model, the yield surface changes size uniformly in all directions such that the yield stress increases (or decreases) in all stress directions as plastic straining occurs.

6.6 Solution times

The Linux-based computer system used for the computations consisted of four Intel Xeon X7460 2.67 GHz chips, each containing 6 processor cores, giving a total of 24 available processor cores. However, due to Abaqus software licensing limitations, only 6 of the available cores were able to be used in parallel. The time taken to obtain a solution for the tension loading case with the present degree of mesh refinement and number of load increments was about 80 minutes. This averaged out to 4.0 minutes per load increment, where approximately the last half of the series of the load increments involved plasticity. In comparison, the computation time taken per load increment for the compression loading case was about 3.7 minutes.

7. Elasto–plastic 3D finite element contact analysis results

In this section, the results from the 3D Abaqus elasto–plastic finite element analyses are presented. Under the applied uniaxial-loading conditions, the material stress–strain response is linear until the material yield stress is reached, after which the response becomes nonlinear in the elasto–plastic regime. A state of general triaxial stress exists (with direct stresses σ_{xx}, σ_{yy}, and σ_{zz}, and shear stresses τ_{xy}, τ_{yz}, and τ_{zx}). The von Mises yield criterion was chosen to define the onset of yielding, as Hill [17] has reported that it shows good agreement with the yielding mechanisms typically exhibited by ductile metals.

In plasticity theory, an equivalent (von Mises) stress at a point is defined as

$$\begin{aligned}\sigma_{vm} &= \frac{1}{\sqrt{2}}\sqrt{(\sigma_1-\sigma_2)^2+(\sigma_2-\sigma_3)^2+(\sigma_3-\sigma_1)^2} \\ &= \frac{1}{\sqrt{2}}\sqrt{(\sigma_{xx}-\sigma_{yy})^2+(\sigma_{yy}-\sigma_{zz})^2+(\sigma_{zz}-\sigma_{xx})^2+6\tau_{xy}^2+6\tau_{yz}^2+6\tau_{zx}^2}\end{aligned} \tag{9}$$

where σ_1, σ_2, and σ_3 are the principal stresses. Yielding is assumed to occur when $\sigma_{vm} \geq \sigma_{cpl}$ for the material in question, where σ_{cpl} is the material uniaxial true cyclic yield stress and corresponds to the equivalent yield stress. In elasto–plastic analysis procedures, Brombolich [1] has noted that the equivalent stress–equivalent strain relationship is identical to the uniaxial stress–strain relationship. Examination of Equation (9) indicates that it is entirely possible for one of the principal stresses to exceed the uniaxial yield stress and yet have the equivalent stress remain below the equivalent yield stress.

The cyclic stress–strain material properties for aluminium alloy 7050-T74 (see Figure 5) and titanium alloy Ti-6Al-4V (see Figure 6) given in the previous section were used. The cyclic stress–strain behaviour was taken to be the stabilised behaviour. By this it is meant that the stress–strain relationship was assumed to be unaffected by further load cycling.

In order to put the magnitude of the applied load in perspective, consider that local yielding of the empty hole is just starting to occur at a tension load level of P = 15.75 kN. At this load level, the peak von Mises stress in the empty-hole coupon is 277.5 MPa, which is just above the cyclic proportional limit of 276.9 MPa for the 7050-T74 material. The average gross-section stress (hole excluded) is about 88 MPa and the average net-section stress (hole included) is about 111 MPa.

7.1 Tangential stress around edge of empty hole – tension loading

An elasto–plastic 3D finite element analysis of the empty-hole coupon was conducted under the prescribed tension loading conditions. For each load level, P, the peak value of the normalised tangential stress around the boundary of the hole, σ_{tt}/S_{yt}, corresponds to the instantaneous K_t of the hole at that particular load increment. At load levels $P \leq 15.75$ kN, where the response was in the linear-elastic range, the stress concentration factor based on the gross cross-section of the coupon at the hole was determined to be K_t = 3.340 at a point lying on the midplane of the coupon at $(x, y, z) = (\pm 3.175, 0, 0)$.

The variation σ_{tt}/S_{yt} around the boundary of the hole at the midplane of the plate is shown in Figure 20. There the σ_{tt}/S_{yt} response is plotted for increasing load levels, and it always has a peak located at $\theta = 0°$. As the load is progressively increased beyond 15.75 kN, which corresponds to 45% of the maximum load level, the effects of material plasticity come increasingly into play. As a result, the peak value of σ_{tt}/S decreases, and it is also accompanied by a flattening of the peak in the stress distribution.

Figure 21 shows the variation in K_t as a function of applied tension load. Once plasticity begins to occur, the K_t progressively reduces approximately linearly with increasing load. The K_t reduces from its linear-elastic value of 3.340 to its final elasto–plastic value of 2.472 at the maximum tension load of P = 35 kN. The corresponding plastic zone is approximately 2.4 mm deep in a radial direction at the midplane of the plate. This increases to approximately 3.5 mm at the free surface. This is in keeping with known behaviour, wherein the size of the plastic zone under the greater constraint of plane strain–like conditions at the midplane is less than that which occurs under plane stress–like conditions at the outer surface. Furthermore, the continuous reduction in K_t that is displayed here is consistent with the behaviour reported by Theocaris and Marketos [6], where an elastic–plastic analysis of a uniaxially-loaded thin narrow strip of a strain-hardening material perforated with a circular hole was conducted.

The stress concentration results as obtained here can be compared to a handbook 2D linear-elastic solution obtained using Equation (5). For the present coupon geometry, W = 30 mm and d = 6.35 mm, and so the 2D value of K_t is 3.168. This compares favourably with the 3D graded-mesh FEA result obtained in the linear-elastic response region of K_t = 3.340, which is only 5.4% higher. By applying the inverse of the 2D FWC factor, we obtain a 3D infinite-plate

peak value of K_t = 3.163, which is only 0.4% less than the peak K_t value of 3.175 obtained by interpolating the results presented by Folias and Wang [14]. This provides us with some measure of confidence in the present 3D FEA results.

The maximum value of compression load is P = 14 kN, and at this load level there is no local yielding of the empty hole. The peak von Mises stress is 246.7 MPa, which is 10.9% less than the stress at the limit of proportionality, so the response under compression loading is entirely linear elastic in its behaviour. This means that the compressive K_t for the compression empty-hole case is constant at 3.340, which is the same as that of the tensile K_t for the tension-loaded empty-hole case in the linear-elastic response regime.

7.2 Stress around edge of hole with pin – tension loading

An elasto–plastic 3D finite element contact analysis of the aluminium coupon with the titanium pin inserted into the hole was conducted under the prescribed tension loading conditions, where a maximum load of P = 35 kN was applied to the coupon. The stress distribution around the hole was found to remain linear-elastic up to a load of P = 15.75 kN, beyond which plastic deformation occurred.

Figure 22 shows a series of stress contour plots for hole–pin contact conditions corresponding to remote uniaxial tension load levels of 15.75 kN, 17.5 kN, 21.0 kN, 28.0 kN and 35.0 kN. The contour plots labelled (a)–(e) give the results for the tangential stress σ_{tt} = S22. Contour plots (f)–(j) show the von Mises stresses in the plastic zone, where the colour contours have been configured to display only those von Mises stresses that exceed the cyclic proportional limit of σ_{cpl} = 276.89 MPa of the aluminium alloy. In Figure 22f, there is a very small region where the von Mises stress exceeds the proportional limit of the material, which indicates that the load level of P = 15.75 kN is more or less at the limit of the linear-elastic response regime; beyond this point the stress response around the boundary of the hole will be elasto–plastic in nature.

Figure 23 shows a series of stress contour plots of the von Mises stress in the plastic zone for hole–pin contact conditions corresponding to remote uniaxial tension load levels of 21.0 kN, 24.5 kN, 28.0 kN, 31.5 kN and 35.0 kN (60%–100% of the maximum tension load in increments of 10%). The colour contours have been configured to clearly show the extent of the plastic zone by displaying only those von Mises stresses that exceed the cyclic proportional limit of σ_{cpl} = 276.89 MPa of the aluminium alloy. The plots labelled (a)–(e) give the results for von Mises stress occurring on the free surface of the coupon, while plots (f)–(j) show the von Mises stress occurring at the midplane surface of the coupon. The nominal 19.6° extent of the contact arc is as indicated (this is further discussed below).

7.2.1 Evolution of plastic zone with applied load

From an inspection of the series of plots shown in Figure 23, which show the evolution of the plastic zone with increasing tension load, it is evident that the cross-sectional area of the plastic zone is somewhat greater at the midplane surface than at the free surface of the coupon. This is the *reverse* of what normally happens when the hole is empty, where the reduced constraint corresponding to the conditions of plane stress at the free surface causes the size of the plastic zone to be larger at the free surface than at the midplane location.

The variation in the depth of the plastic zone, d_p, as a function of the tension applied load was investigated. Figure 24 shows the variation in normalised plastic zone depth d_p/r along the x-axis at both the midplane surface and the free surface of the coupon, where r is the radius of the hole. Once plasticity begins to occur, it is apparent that the depth of the plastic zone increases approximately linearly with increasing load, with the growth rate being marginally higher at the midplane of the coupon. At the maximum load, the depth of the plastic zone is approximately 76.2% of the hole radius, with d_p/r = 0.762 (d_p = 2.42 mm) at the midplane surface and d_p/r = 0.630 (d_p = 2.00 mm) at the free surface. In comparison, the results for the empty-hole case were d_p/r = 0.756 (d_p = 2.40 mm) at the midplane surface and d_p/r = 1.102 (d_p = 3.50 mm) at the free surface.

At any vertical cross-section (on planes parallel to the x-y plane), if the total combined area of the left-hand and right-hand plastic zones is denoted by A_p, and noting that the area of the hole is πr^2 (= 31.67 mm^2), then the normalised area of the plastic zones can be defined as $A_p/(\pi r^2)$. The variation in $A_p/(\pi r^2)$ as a function of the tension applied load at both the midplane surface and free surface of the coupon is shown in Figure 25. At the maximum load, the total cross-sectional area of the plastic zones at the midplane surface is A_p = 20.22 mm^2, which is equivalent to 63.8% of the area of the hole ($A_p/(\pi r^2)$ = 0.638), indicating that a substantial degree of plastic deformation has occurred. In comparison, the area of the plastic zones at the free surface is about 20% smaller than that at the midplane surface. Once plastic deformation has been initiated, the increase in area of the plastic zones displays a power-law behaviour with increasing load, with an exponent of approximately 2.

7.2.2 Variation of radial stress with applied load

For the filled-hole case, the variation of the normalised radial stress, σ_{rr}/S_{yt}, around the boundary of the hole at the midplane of the plate and a range of tension load levels is shown in Figure 26. The parameter σ_{rr}/S_{yt} corresponds to the contact pressure developed at the hole–pin interface, and takes on a parabolic shape that is typical of many contact problems. The response obtained here is qualitatively similar to that which has been reported elsewhere by Karami [7] and Martín and Aliabadi [8].

By identifying the point where σ_{rr}/S_{yt} = 0, the contact angle at the midplane is estimated to be approximately η_t = 19.6°, and it also appears to be nominally independent of load level. The fact that the computed contact stress overshoots the expected value of zero at the end of the contact arc is an artefact of the mesh discretisation and the high stress gradients occurring in this region. However, as the contact pressure is at its lowest level in this region, it is considered that additional mesh refinement is unwarranted.

From the family of response curves shown in Figure 26, it is evident that the peak in the σ_{rr}/S_{yt} response always occurs at θ = 0°, and it reaches a maximum amplitude of σ_{rr}/S_{yt} = –0.758. This maximum applies throughout the linear-elastic response regime. Once plasticity begins to occur around the hole in the hole–pin contact region, the peak value of σ_{rr}/S_{yt} progressively reduces in magnitude with increasing load level. The variation in the peak value of σ_{rr}/S_{yt} as a function of load is shown in Figure 27. At the maximum load of P = 35 kN, it has reached a value of σ_{rr}/S_{yt} = –0.631, which is a reduction of about 16.8% compared to the value in the linear-elastic response region.

7.2.3 *Variation of tangential stress with applied load*

The variation of the normalised tangential stress, σ_{tt}/S_{yt}, around the boundary of the filled hole at the midplane of the plate and a range of tension load levels is shown in Figure 28. The response obtained here is qualitatively similar to that which has been reported elsewhere by Karami [7] and Martín and Aliabadi [8]. At any given load level, the peak value of σ_{tt}/S_{yt} corresponds to the K_t for the hole–pin combination. The values of σ_{tt}/S_{yt} in the vicinity of the peak are affected by mesh density in that region, with the rounded nature of the peak being typical of smoothing effects related to the moderate level of mesh refinement that was used. Going by the results presented in [9], it is anticipated that the magnitudes of the peaks at the various load levels may be underestimated in the present analysis by less than 1%, and that the locations of the peaks may be subject to a position error of the order of 0.5° or so.

At load levels $P \leq 15.75$ kN, where the response is purely linear-elastic in nature, the tensile K_t was determined to be $K_t = 3.005$ at a point lying on the midplane of the coupon at an angle of $\theta = \eta_t = 19.6°$ on the hole boundary. This value of K_t is about 11% lower than the result obtained for this geometry for the empty-hole case. At $\theta = 0°$ it was determined that $K_t = 2.715$, which is about 10% lower than that which occurs at $\theta = \eta_t$. The corresponding compressive K_t at the hole boundary was determined to be $K_t = -0.927$, at a point lying on the midplane of the coupon at $\theta = \pm 90°$.

As for the empty-hole case, once the load exceeds $P = 15.75$ kN, the response curves shown in Figure 28 indicate clearly that material plasticity begins to come into play, with the peak value of σ_{tt}/S_{yt} decreasing with increasing levels of plasticity as the load level increases. The location of the peak value remains constant at $\theta = 19.6°$. At the maximum load of $P = 35$ kN, the tensile K_t at the midplane was determined to be $K_t = 2.377$ at the $\theta = \eta_t = 19.6°$ location, while at $\theta = 0°$ it was determined that $K_t = 1.943$, which is about 18% lower than that at $\theta = \eta_t$. From this, it is apparent that plastic deformation causes a much greater relative reduction in the stresses at the $\theta = 0°$ location than at the $\theta = \eta_t$ location. This is likely to be related to the fact that the peak in the contact pressure is located at $\theta = 0°$. As the peak tangential stress occurs at the $\theta = \eta_t = 19.6°$ location on the hole boundary, it could be expected that fatigue cracking is more likely to initiate in that vicinity rather than at the $\theta = 0°$ position.

The peak von Mises stress at the midplane of the coupon at the maximum tension load $P = 35$ kN is $\sigma_{vm} = 447.8$ MPa, and this corresponds to a true plastic strain of magnitude $\varepsilon_p = 0.005342$ mm/mm. The plastic zone extends along the boundary of the hole to approximately $\theta = 39.4°$, which is about twice the extent of the contact arc itself, which nominally finishes by $\theta = \eta_t = 19.6°$. At the same time, the peak von Mises stress in the pin is 129.1 MPa. This stress is quite low in magnitude and is well within the linear-elastic range of the titanium alloy Ti-4Al-6V material. As a result, no plasticity is occurring in the pin, even though there is significant plasticity occurring around the boundary of the hole in the coupon.

7.2.4 *Variation of K_t with applied load*

The variation of the tensile and compressive values of peak K_t with increasing magnitude of applied tension and compression load levels is shown in Figure 29. For the tension applied loading, the gradual reduction in tensile K_t after the onset of plasticity for load levels $P >$

15.75 kN is readily apparent. The K_t reduces from its linear-elastic value of 3.005 to its final elasto–plastic value of 2.377 at the maximum tension load P = 35 kN, a total reduction of about 24%. On the other hand, the compressive K_t increases slightly in magnitude from a value of K_t = –0.927 to K_t = –0.984 for the tension applied loading, an increase of about 6%. For the compression applied loading case, Figure 29 shows that the compressive K_t = –1.810 and the tensile K_t = 0.771, and these values remain constant throughout the loading range, as the material response never enters the elasto–plastic regime.

The midplane tensile and compressive K_t values determined for the tension loading case for the range of load level increments that were used are given in Table 6 for angles $\theta = 0°$, $\theta = \eta_t = 19.6°$ and $\theta = 90°$.

7.3 Comparison of filled-hole and empty-hole cases – tension loading

We now proceed to compare the tangential stress responses for the neat-fit filled-hole case (Figure 28) with those obtained for the coupon with an empty hole (Figure 20). In the linear-elastic response range, the K_t of the filled hole is approximately 10% lower than that of the empty hole for the tension applied loading. It is interesting to note that the linear-elastic load limit is approximately the same as that found in the analysis of the empty-hole case. This is because of the presence of significant radial stresses that are developed as a result of the contact pressure that is occurring in the region of hole–pin contact surface interaction.

In order to study the effectiveness of the filled hole relative to that of the empty hole, we define a parameter Ψ, which is equal to the ratio of the K_t of the filled hole to the K_t of the empty hole:

$$\Psi = \frac{K_t\big|_{filled\ hole}}{K_t\big|_{open\ hole}} \tag{7}$$

The variation in the value of Ψ as a function of the applied tension load P is shown in Figure 30. It is evident that Ψ is constant at a value of Ψ = 0.900 in the linear-elastic load range $0 \le P \le 15.75$ kN. This indicates that hole–pin contact is quite effective in reducing the K_t of the hole. For loads above 15.75 kN, with their attendant plasticity around the hole boundary, the parameter Ψ increases slowly with load to a value of Ψ = 0.962 at the maximum load of P = 35 kN. This indicates that the pin is progressively less effective in reducing the K_t at the higher loads in the elasto–plastic response range than it is in the linear-elastic response range.

If we now use the averaged tangential stress at the midplane for the filled-hole and open-hole cases, instead of the K_t values, taken over the region $0° \le \theta \le 22°$, the resulting hole effectiveness response parameter Ψ is shown in Figure 31. In the linear-elastic response range, the filled-hole case produces averaged tangential stresses that are about 11% lower than those of the empty hole, with Ψ = 0.890, which is almost the same value that was obtained for the Ψ response based on K_t. In the elasto–plastic response regime, Ψ continues to slowly reduce, reaching a 3.3% lower value of Ψ = 0.861 at the maximum applied load. This indicates that the pin is progressively more effective in redistributing the tangential stresses as the load is increased, even though it becomes less effective in reducing the K_t.

7.4 Stress around edge of hole with pin – compression loading

The variation of the normalised radial stress, σ_{rr}/S_{yc}, around the boundary of the hole at the midplane of the plate under compression loading is shown in Figure 32. This curve applies to the response for the full range of compression loading, 0 kN ≤ P ≤ 14 kN, as the response is purely linear elastic in nature within this compression load range. By identifying the point where $\sigma_{rr}/S_{yc} = 0$, the contact arc is estimated to cover the range 36° ≤ θ ≤ 90° at the midplane. Hence, the contact angle under compression loading is approximately η_c = 54.0° in extent, and it is independent of load level. The fact that the value of contact stress overshoots the expected value of zero at the end of the contact arc is an artefact of the mesh discretisation and the high stress gradients occurring in this region. The peak in the σ_{rr}/S_{yc} response occurs at θ = 90°, reaching a maximum amplitude of $\sigma_{rr}/S_{yc} = -1.477$.

Figure 33 shows the corresponding variation in the normalised tangential stress, σ_{tt}/S_{yc}, around the boundary of the hole at the midplane of the plate. The value of σ_{tt}/S_{yc} increases from a compressive peak value of $\sigma_{tt}/S_{yc} = -1.810$ at θ = 0°, to a tensile peak value of σ_{tt}/S_{yc} = 0.771 at θ = 90°. The curve includes a small inflection point at about θ = 36°, which coincides with the boundary of the hole–pin contact region. These two peak values are significantly less than those obtained for the empty-hole case under compression loading, which are a compressive peak value of $\sigma_{tt}/S_{yc} = -3.340$ at θ = 0° and a tensile peak value of σ_{tt}/S_{yc} = 1.285 at θ = 90°. Under the compression loading, the ratio of the K_t value of the filled hole to the K_t of the empty hole is constant over the full load range, with the value for the compressive K_t being Ψ = 0.542 (see Figure 30) and the value for the tensile K_t being Ψ = 0.600.

The tensile and compressive K_t values determined for the compression loading case for a range of load level increments are given in Table 6 for points at angular locations θ = 0° and θ = 90°.

7.5 Stress around edge of hole with pin – comparison with 2D linear-elastic analytical solution

In a conference paper published in 1964, Wilson [11] provided an analytical/numerical solution to the general 2D contact problem of an elastic infinite plate loaded by stresses S_x and S_y at infinity and containing a smooth elastic circular insert of a different material. The solution method involves an iterative procedure and, although it was described as approximate, Wilson's comparisons with known analytical solutions for some special cases appear to indicate that it is nonetheless very accurate. In prior work by Waldman [9], a FORTRAN program implementing Wilson's method was written. This program was utilised here to compute predictions of the radial stresses σ_{rr} and tangential stresses σ_{tt} occurring around the boundary of the hole for comparison with the FEA results in the linear-elastic response regime. The elastic material properties for aluminium alloy 7050-T74 and titanium alloy Ti-6Al-4V were used when computing the stress response to load cases corresponding to uniaxial tension and uniaxial compression.

7.5.1 *Tension loading*

For the tension-loaded filled-hole case in the linear-elastic response regime, Figure 34 shows a comparison of the 2D analytical predictions and the 3D FEA results for the normalised radial stress σ_{rr}/S_{yt} around the boundary of the hole at the midplane of the plate. The contact angle predicted by the 2D analytical solution is $\eta_t = 19.2°$, which agrees very closely with the value $\eta_t = 19.6°$ estimated from the 3D FEA. The results for the normalised tangential stress σ_{tt}/S_{yt} are shown in Figure 35. The agreement between the analytical and FEA results for the distributions of σ_{rr}/S_{yt} and σ_{tt}/S_{yt} is generally quite good. In the region $0° \le \theta \le 25°$, the FEA results are approximately uniformly greater than the 2D analytical predictions by 7.5% or so. The fact that the FEA results produce somewhat higher peak stresses can be explained by the fact that the 2D solution is for an infinite plate, while the FEA solution involves not only a finite-width plate but one with finite thickness that develops 3D through-thickness effects. In the previous section involving the analysis of the empty-hole case, it was determined that the 3D FEA results were some 5.4% higher than the handbook solution based on 2D theory. Hence, by scaling the results from the 2D analytical solution by a factor of 1.054 to account for finite-width effects, it would be possible to obtain a much improved agreement between the analytical 2D results and the 3D FEA results.

7.5.2 *Compression loading*

For the compression-loaded filled-hole case in the linear-elastic response regime, Figure 36 shows a comparison of the 2D analytical predictions and the 3D FEA results for the normalised radial stress σ_{rr}/S_{yc} around the boundary of the hole at the midplane of the plate. The contact angle predicted by the 2D analytical solution is $\eta_c = 53.9°$, which agrees very closely with $\eta_c = 54.0°$ obtained from the 3D FEA. Here we find that the analytical and FEA results for the contact pressure distribution are in excellent agreement, even without the additional application of any finite-width correction to the 2D results. This might be due to the fact that the size of the contact region is much greater for the compression loading than it is for the tension loading, possibly resulting in some kind of restraint that reduces the influence of any finite-width effects at the midplane of the coupon.

The results for the normalised tangential stress σ_{tt}/S_{yc} for the compression-loaded filled-hole case are shown in Figure 37. In line with the results obtained above for σ_{rr}/S_{yc}, these too show that the analytical and FEA solutions are in good agreement. However, it is very apparent that the spacing of the finite elements in the vicinity of the edge of the contact arc is insufficiently fine to resolve the very sharp local maximum in the σ_{tt}/S_{yc} stress response that occurs in the vicinity of $\theta = 36°$. As a result, the FEA solution has produced a broader and smoothed out local maximum in the σ_{tt}/S_{yc} stress response in that region.

7.6 Stress decay at minimum cross-section for hole with pin

To assist in understanding fatigue cracking behaviour, it is often useful to have some knowledge of the decay of stresses along potential crack paths. For the hole fitted with the pin, the variation of the normalised tangential stress σ_{tt}/S_{yt} versus the distance away from the hole centre normalised by the hole radius, x/r, is shown in Figure 38 for $1.0 \le x/r \le 2.5$ and a range of tension load levels. The results obtained from the linear-elastic analysis of the

empty hole are also shown for reference. Overall, it is evident that σ_{tt}/S_{yt} decays away very rapidly with increasing distance from the hole edge. The linear-elastic results for the empty hole show a somewhat greater initial rate of decay. It is notable that at higher load levels the eventual overall decay is preceded by a short region where the stress is increasing away from the hole edge, before eventually decaying away. At a distance one radius away from the hole edge (x/r = 2.0), the tangential stress has been reduced to between 131% and 135% of the gross-section average stress, depending on the load level.

As determined earlier for the hole fitted with the pin, the response is elasto–plastic in nature for load levels P > 15.75 kN. It is evident from Figure 38 that the peak normalised stress reduces as the amount of plastic deformation increases. This results in a redistribution of this stress such that each elasto–plastic σ_{tt}/S_{yt} response curve crosses over the linear-elastic response curve and has some portion of its response lying above the linear-elastic response curve. It is also worth noting that, at the maximum load level of P = 35 kN, the peak in σ_{tt}/S_{yt} occurs at x/r = 1.18, which is slightly in from the edge of the hole. At this location, σ_{tt}/S_{yt} = 2.122, while at x/r = 1.00 the value is σ_{tt}/S_{yt} = 1.943, which is about 8% lower. The response peak at the load level P = 28 kN has a similar characteristic. This behaviour comes about as a result of plasticity effects. However, at lower load levels, the peak stress occurs at the hole edge for both the linear-elastic and elasto-plastic response regimes.

8. Conclusion

The LIF Hawk Filled Hole Coupon, which is a uniaxially-loaded fatigue test coupon made from aluminium alloy plate that has a low-clearance titanium alloy pin inserted into a centrally-located hole, was the subject of extensive 3D FEA investigations. These utilised the contact analysis capabilities of the Abaqus FEA code in conjunction with its elasto–plastic analysis capabilities.

The linear-elastic analysis reported here provides useful engineering data concerning the K_t behaviour when hole–pin contact occurs, considering both load magnitude and hole–fastener clearance. A range of gaps from 0 mm to 0.01 mm were investigated for load levels representative of those used during fatigue testing of these coupons. A reduction in the K_t occurred because, upon contact of the edge of the hole with the fastener, load transfer between the fastener and the plate occurs in the transverse direction under a tensile load, propping open the hole.

A detailed 3D elasto–plastic FEA investigation has also been conducted, using representative cyclic elasto–plastic stress–strain material data for the plate and the pin. The analyses involved separate consideration of cases of tension and compression loading. The K_t values determined for these loading cases for the range of load levels used in the fatigue testing program have been presented in Table 6. For validation purposes, this analysis work was supplemented by a 2D linear-elastic analysis based on a previously published analytical solution that had recently been implemented by the author.

The specified tension loading range for the fatigue test coupon that was applied during the fatigue testing program was 0 kN ≤ P ≤ 35 kN. For the filled-hole coupon, the computed response to this loading was found to remain linear-elastic in its behaviour for loads where P

≤ 15.75 kN, with a tensile-stress peak of K_t = 3.005 and a compressive-stress peak of K_t = –0.927. The hole–pin contact arc angle was determined to be η_t = 19.6° in the linear-elastic response regime, with the contact region extending between –19.6° ≤ θ ≤ +19.6° and –160.4° ≤ θ ≤ +160.4° on the two sides of the hole. This is in excellent agreement with the 2D analytical results that were also computed. The response became elasto–plastic for the tension loading for P > 15.75 kN. At the maximum applied tension load of P = 35 kN, the tension-stress peak K_t was reduced in value to K_t = 2.377 (–21%) and the compressive-stress peak K_t increased in magnitude somewhat to K_t = –0.984 (+6%). Interestingly, the hole–pin contact angle remained at η_t = 19.6° throughout the elasto–plastic response regime, the same as that in the linear-elastic response regime. At the maximum tension load, the normalised maximum cross-sectional area of the plastic zones was $A_p/(\pi r^2)$ = 0.638 at the midplane surface of the filled-hole coupon.

The analysis of the empty-hole coupon has also determined that the elasto–plastic material deformation that occurs at the higher tension loads reduces the K_t of the empty-hole coupon. The empty-hole peak K_t reduces from K_t = 3.340 in the linear-elastic response regime to a value of K_t = 2.472 at the maximum load in the elasto–plastic response regime. This is a very significant reduction of about 26%, and occurs in an approximately linear manner. The depth of the plastic zone was also determined to be greater in the empty-hole coupon than the filled-hole coupon. Interestingly, it was found that the tension-load linear-elastic limit for the empty-hole coupon was approximately the same as for the filled-hole coupon when a zero-clearance insert is used.

For the filled-hole coupon, at the maximum tension load the peak K_t that was computed was only 3.8% less than the K_t obtained for the empty hole at this same load level, while in the linear-elastic range it was 10.0% less. This indicates that, due to the local plastic deformation that occurs in the contact zone, the zero-clearance fastener becomes progressively less effective in reducing the K_t at the higher loads in the elasto–plastic response range than it is in the linear-elastic response range.

For both the filled-hole and open-hole coupons, it has been determined that the response is entirely linear-elastic in nature over the specified compression loading range that was used during the fatigue testing program, 0 kN ≤ P ≤ 14 kN. For the filled-hole coupon, it results in a constant tensile-stress peak K_t = 0.771 and a constant compressive-stress peak K_t = –1.810. The hole–pin contact arc angle for the compression loading was computed to be η_c = 54.0° using 3D FEA, and this was in good agreement with the 2D analytical results that were also computed.

For the filled-hole coupon, as the locations of the peak tangential stresses occurred at four points around the hole boundary, at θ = ±19.6° and θ = ±160.4°, it may be more likely for fatigue cracking to initiate in the vicinity of those locations, rather than at the two θ = 0° and θ = 180° positions of peak stress that arise for an open hole coupon. However, this is open to conjecture at this point in time, as it is anticipated that any fatigue cracking that occurs will be subject to the influence of any existing local manufacturing or material defects that may be present in the bore of the hole.

For the empty-hole case under the tension loading, it is known that the cross-sectional area of the plastic zone around the hole varies through the thickness, and is greater on the free surface of the fatigue test coupon than at the midplane surface. This is consistent with the transition from a state of plane stress at the surface to one which approaches a more constrained state of plane strain at the midplane. However, when an elastic neat-fit insert is placed into the hole, it was found that the previously described behaviour is reversed. With the insert fitted into the hole, the cross-sectional area of the plastic zone was determined to be considerably greater at the midplane of the coupon than at the free surface of the coupon (by about 25% at the maximum load level).

Having completed an elasto–plastic 3D FEA of the contact interaction that is occurring at the hole–pin interface in the LIF Hawk Filled Hole Coupon during fatigue testing, it would be useful to introduce a crack into the structure in the presence of the existing plastic zone. Analyses conducted using more complex, but potentially more accurate, material plasticity models (e.g. kinematic hardening, where a translation of the yield surface in stress space occurs) may also be worthwhile and prove to be instructive.

9. References

1. LJ Brombolich. Elastic-plastic analysis of stresses near fastener holes. AIAA Paper No. 73-252, AIAA 11th Aerospace Sciences Meeting, Washington DC, 10–12 January 1973.

2. JH Crews Jr. An elastoplastic analysis of a uniaxially loaded sheet with an interference fit bolt. NASA Technical Note TN D-7748, National Aeronautics and Space Administration, Washington, October 1974.

3. DL Rich, LF Impellizzeri. Fatigue analysis of cold-worked and interference fit fastener holes. Cyclic Stress–Strain and Plastic Deformation Aspects of Fatigue Crack Growth, ASTM STP637, LF Impellizzeri (Editor), American Society for Testing and Materials, 1977, pp. 153–175.

4. RP Carey. Three-dimensional computation of stress, strain and strain energy density under interference-fit and after cold-working of holes. Technical Memorandum ARL-STRUC-TM-478, Aeronautical Research Laboratory, Defence Science and Technology Organisation, Department of Defence, Australia, January 1988.

5. D Duprat, D Campassens, M Balzano, R Boudet. Fatigue life prediction of interference fit fastener and cold worked holes. International Journal of Fatigue, Vol. 18, No. 8, 1996, pp. 515–521.

6. PS Theocaris, E Marketos. Elastic–plastic analysis of perforated thin strips of a strain-hardening material. Journal of the Mechanics and Physics of Solids, Vol. 12, No. 6, 1964, pp. 377–390.

7. G Karami. Boundary element analysis of elasto-plastic contact problems. Computers & Structures, Vol. 41, No. 5, 1991, pp. 927–935.

8. D Martín, MH Aliabadi. Boundary element analysis of two-dimensional elastoplastic contact problems. Engineering Analysis with Boundary Elements, Vol. 21, Issue 4, 1998, pp. 349–360.

9. W Waldman. Linear-elastic 2D and 3D finite element contact analysis of a hole containing a circular insert in a fatigue test coupon. Technical Report, Aerospace Division, Defence Science Technology, Department of Defence, Australia, 2015.

10. M Stippes, HB Wilson Jr, FN Krull. A contact problem for a smooth disk in an infinite plate. Proceedings of the Fourth US National Congress of Applied Mechanics, Vol. 2, pp. 799–806, 1962.

11. HB Wilson Jr. Approximate determination of contact stresses in an infinite plate with a smooth circular insert. Proceedings of the 2nd Southeastern Conference on Theoretical and Applied Mechanics, 5–6 March 1964, Atlanta, Georgia, USA.

12. MMPDS-03, Metallic Materials Properties Development and Standardization, Federal Aviation Administration, USA, October 2006.

13. WD Pilkey, DF Pilkey. Peterson's Stress Concentration Factors. Third Edition, John Wiley & Sons, Inc., 2008, ISBN: 978-0-470-04824-5.

14. ES Folias, J-J Wang. On the three-dimensional stress field around a circular hole in a plate of arbitrary thickness. Computational Mechanics, Vol. 6, 1990, pp. 379–391.

15. AK Rao. Elastic analysis of pin joints. Computers & Structures, Vol. 9, No. 2, 1978, pp. 125–144.

16. HD Conway, SM Vogel, SM Farnham, S So. Normal and shearing contact stresses in indented strips and slabs. International Journal of Engineering Science, Vol. 4, No. 4, 1966, pp. 343–359.

17. R Hill. The Mathematical Theory of Plasticity. Oxford at the Clarendon Press, First Edition, 1950.

Table 1: *Cyclic true stress–strain data for aluminium alloy 7050-T74.*

True Strain, ε (mm/mm)	True Stress, σ (MPa)
0.000000	0.00
0.000500	34.49
0.001000	69.02
0.001499	103.58
0.001747	120.87
0.001998	138.17
0.002246	155.48
0.002397	172.78
0.002745	190.13
0.002996	207.46
0.003195	221.34
0.003423	242.14
0.003726	259.52
0.003992	276.89
0.005467	345.24
0.006482	380.98
0.007678	409.23
0.008916	426.43
0.011694	447.15
0.015991	469.40
0.020342	486.22
0.027604	503.94
0.035340	514.28
0.061848	528.83

Table 2: *Cyclic true stress–strain data for titanium alloy Ti-4Al-6V (STA) L.*

True Strain, ε (mm/mm)	True Stress, σ (MPa)
0.00000	0.00
0.00122	144.03
0.00242	278.00
0.00375	410.24
0.00508	531.24
0.00640	640.04
0.00783	731.88
0.00931	800.83
0.01083	852.81
0.01241	891.84
0.01399	924.38
0.01557	952.44
0.01714	976.64
0.01875	998.57
0.02035	1019.94
0.02198	1039.38
0.02364	1056.48
0.02527	1074.76
0.02689	1089.72
0.02851	1102.95
0.03020	1115.92

Table 3: *Cyclic true plastic stress–strain data for aluminium alloy 7050-T74 for use with Abaqus FEA program, obtained using cubic spline interpolation.*

True Plastic Strain ε_p (mm/mm)	True Stress σ (MPa)
0.000000	276.89
0.000100	292.39
0.000200	307.49
0.000300	321.78
0.000400	334.87
0.000500	346.35
0.000600	355.99
0.000700	364.01
0.000800	370.72
0.000900	376.46
0.001000	381.52
0.001200	390.44
0.001400	398.01
0.001600	404.39
0.001800	409.77
0.002000	414.31
0.002500	422.90
0.003000	429.17
0.003500	434.33
0.004000	438.64
0.004500	442.32
0.005000	445.60
0.005500	448.71
0.006000	451.75
0.006500	454.71
0.007000	457.60
0.007500	460.41
0.008000	463.13
0.008500	465.76
0.009000	468.30
0.009500	470.73
0.010000	473.05
0.011000	477.42
0.012000	481.41
0.013000	485.07
0.014000	488.43
0.015000	491.50
0.016000	494.30
0.017000	496.87

True Plastic Strain ε_p (mm/mm)	True Stress σ (MPa)
0.018000	499.21
0.019000	501.35
0.020000	503.31
0.021000	505.11
0.022000	506.76
0.023000	508.28
0.024000	509.68
0.025000	510.98
0.026000	512.18
0.027000	513.30
0.028000	514.36
0.029000	515.36
0.030000	516.30
0.031000	517.20
0.032000	518.05
0.033000	518.85
0.034000	519.61
0.035000	520.33
0.036000	521.01
0.037000	521.65
0.038000	522.25
0.039000	522.82
0.040000	523.36
0.041000	523.87
0.042000	524.35
0.043000	524.81
0.044000	525.24
0.045000	525.66
0.046000	526.05
0.047000	526.43
0.048000	526.79
0.049000	527.14
0.050000	527.47
0.051000	527.80
0.052000	528.12
0.053000	528.44
0.054000	528.76
0.054223	528.83

Table 4: *Cyclic true plastic stress–strain data for titanium alloy Ti-6Al-4V (STA) L for use with Abaqus FEA program, obtained using cubic spline interpolation.*

True Plastic Strain ε_p (mm/mm)	True Stress σ (MPa)	True Plastic Strain ε_p (mm/mm)	True Stress σ (MPa)
0.000000	410.24	0.006500	945.21
0.000010	416.02	0.006800	951.20
0.000020	421.80	0.007100	956.97
0.000040	433.32	0.007400	962.55
0.000060	444.77	0.007700	967.92
0.000080	456.11	0.008000	973.10
0.000100	467.30	0.008300	978.07
0.000120	478.32	0.008600	982.87
0.000140	489.12	0.008900	987.54
0.000160	499.66	0.009200	992.14
0.000180	509.92	0.009500	996.70
0.000200	519.85	0.009800	1001.30
0.000250	543.03	0.010100	1005.92
0.000300	563.83	0.010400	1010.53
0.000350	582.46	0.010700	1015.08
0.000400	599.17	0.011000	1019.55
0.000450	614.20	0.011300	1023.89
0.000500	627.80	0.011600	1028.09
0.000600	651.60	0.011900	1032.12
0.000700	671.80	0.012200	1035.97
0.000800	688.97	0.012500	1039.64
0.000900	703.65	0.012800	1043.11
0.001000	716.36	0.013100	1046.47
0.001100	727.65	0.013400	1049.79
0.001200	738.04	0.013700	1053.17
0.001300	747.78	0.014000	1056.69
0.001400	756.91	0.014300	1060.40
0.001500	765.48	0.014600	1064.22
0.001600	773.54	0.014900	1068.06
0.001700	781.12	0.015200	1071.81
0.001800	788.28	0.015500	1075.38
0.001900	795.05	0.015800	1078.71
0.002000	801.48	0.016100	1081.82
0.002300	819.01	0.016400	1084.78
0.002600	834.20	0.016700	1087.61
0.002900	847.42	0.017000	1090.37
0.003200	859.06	0.017300	1093.09
0.003500	869.42	0.017600	1095.77
0.003800	878.80	0.017900	1098.41
0.004100	887.47	0.018200	1101.01
0.004400	895.71	0.018500	1103.57
0.004700	903.66	0.018800	1106.09
0.005000	911.33	0.019100	1108.57
0.005300	918.70	0.019400	1111.04
0.005600	925.76	0.019700	1113.48
0.005900	932.52	0.019999	1115.92
0.006200	939.00		

***Table 5**: Values of RGB colour coordinates typically used by MSC Patran for default colours of stress contours.*

Contour Number	Colour	(R, G, B) Colour Coordinates
1	Red	(255, 0, 0)
2	Orange	(255, 119, 0)
3	Yellow	(255, 255, 0)
4	Dark Pink	(255, 0, 255)
5	Light Pink	(255, 191, 255)
6	Dark Green	(0, 127, 0)
7	Light Green	(0, 255, 0)
8	Dark Blue	(0, 0, 170)
9	Light Blue	(0, 153, 255)
10	Cyan	(0, 255, 255)

***Table 6:** K_t values at various angular locations around the hole boundary at the midplane of the plate for the filled-hole coupon for increasing values of remote tension and remote compression loading. Positive and negative K_t values correspond to tensile and compressive stresses, respectively.*

	K_t				
Magnitude of Applied Load (kN)	Remote Tension Loading			Remote Compression Loading	
	$\theta = 0°$	$\theta = \eta_t = 19.6°$	$\theta = 90°$	$\theta = 0°$	$\theta = 90°$
1.75	2.715	3.005	–0.927	–1.810	0.771
3.50	2.715	3.005	–0.927	–1.810	0.771
5.25	2.715	3.005	–0.927	–1.810	0.771
7.00	2.715	3.006	–0.927	–1.810	0.771
8.75	2.714	3.006	–0.927	–1.810	0.771
10.50	2.714	3.006	–0.927	–1.810	0.771
12.25	2.714	3.006	–0.927	–1.810	0.771
14.00	2.714	3.006	–0.927	–1.810	0.771
15.75	2.714	3.006	–0.928	–	–
17.50	2.640	2.999	–0.928	–	–
19.25	2.584	2.935	–0.928	–	–
21.00	2.535	2.871	–0.930	–	–
22.75	2.479	2.822	–0.932	–	–
24.50	2.409	2.775	–0.936	–	–
26.25	2.336	2.719	–0.940	–	–
28.00	2.258	2.655	–0.946	–	–
29.75	2.175	2.586	–0.953	–	–
31.50	2.092	2.518	–0.962	–	–
33.25	2.015	2.447	–0.972	–	–
35.00	1.943	2.377	–0.984	–	–

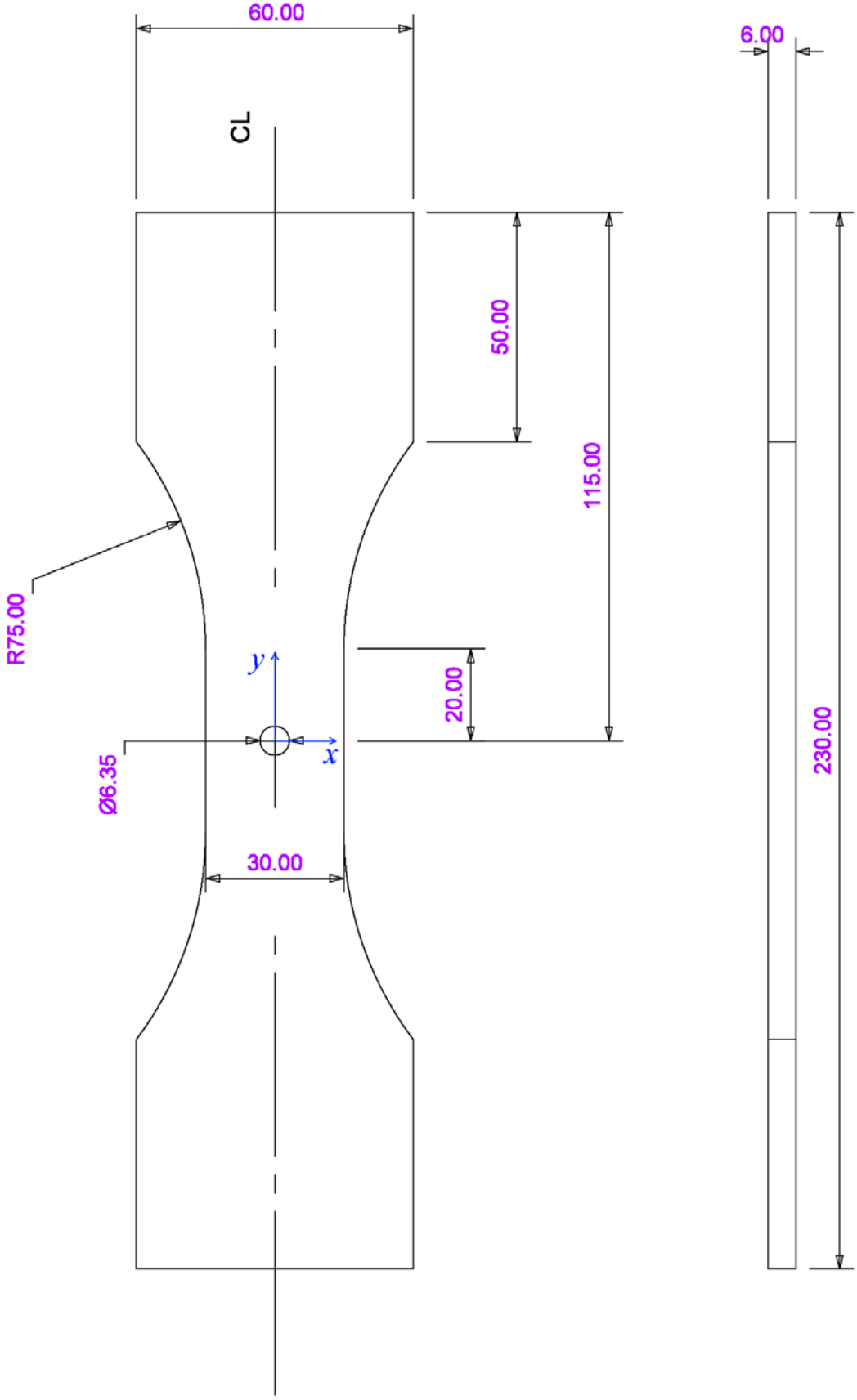

Figure 1: *Drawing showing general dimensions of LIF Hawk Filled Hole Coupon.*

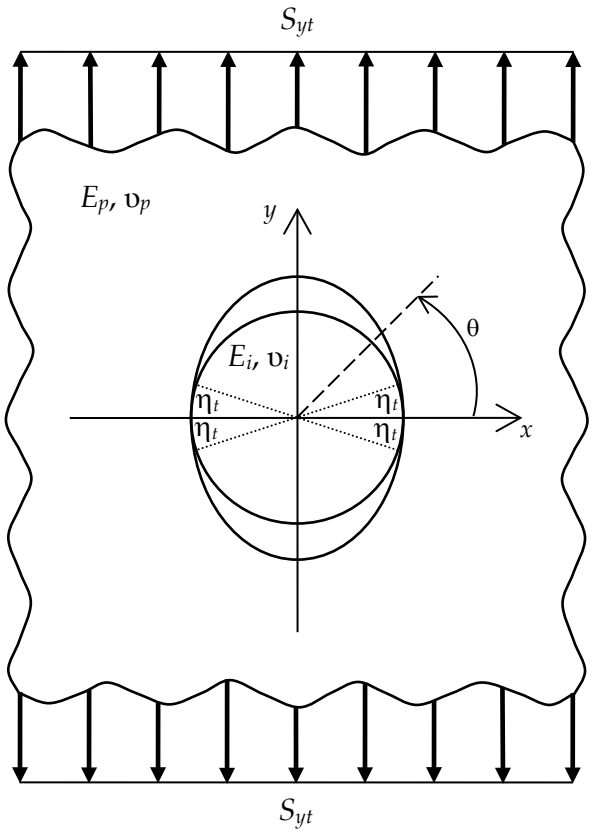

Figure 2: *Geometrical configuration of a plate with a hole loaded by a uniaxial tensile stress* S_{yt} *at infinity showing the contact angle* η_t *between the plate and the circular disk insert.*

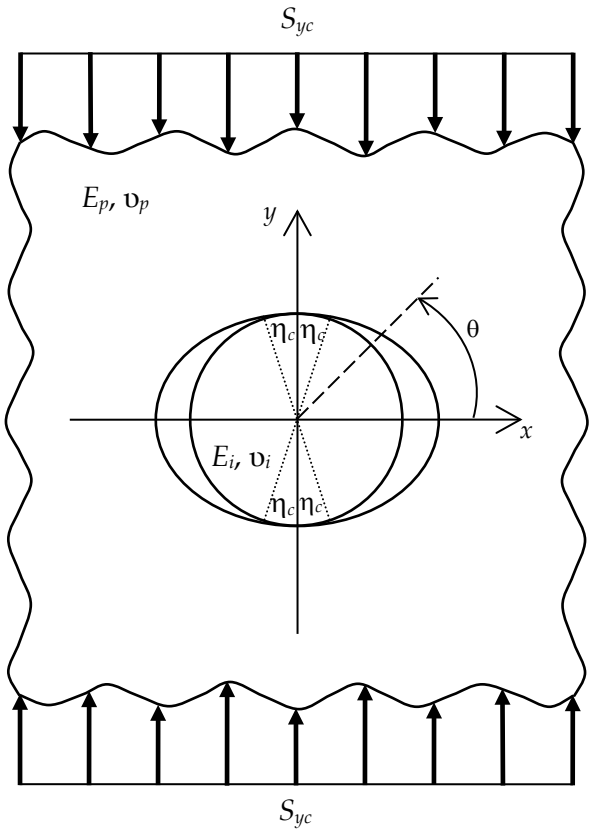

Figure 3: *Geometrical configuration of a plate with a hole loaded by a uniaxial compression stress* S_{yc} *at infinity showing the contact angle* η_c *between the plate and the circular disk insert.*

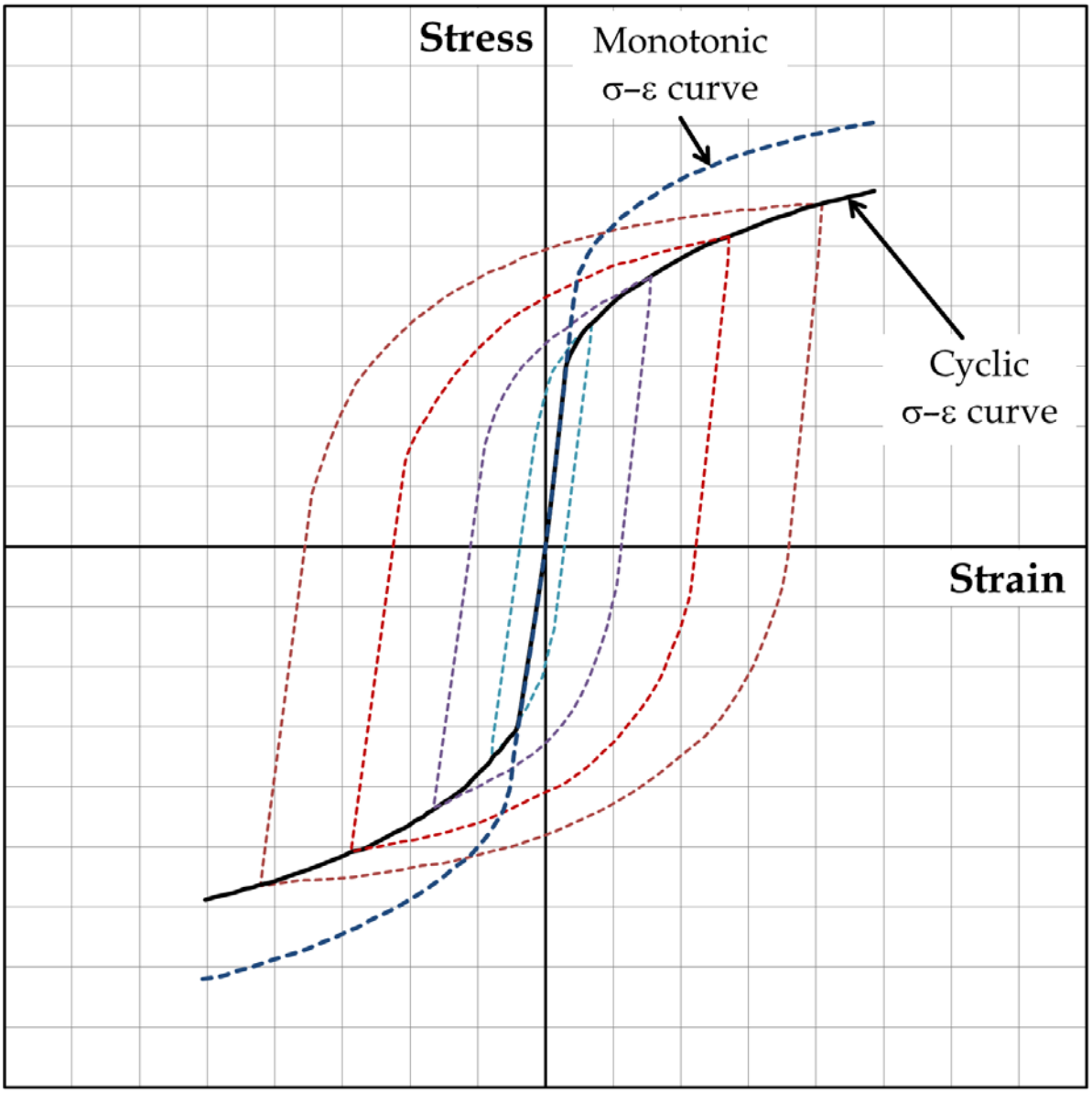

Figure 4: *Cyclic stress–strain curve definition.*

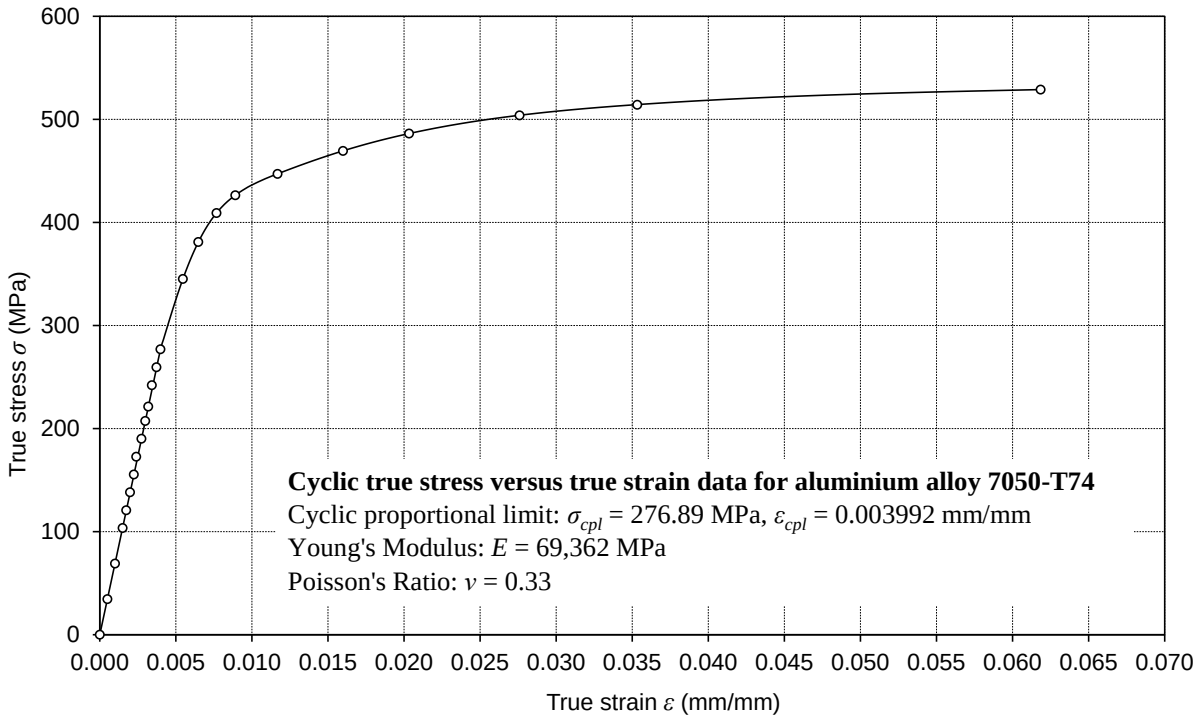

Figure 5: *Cyclic true stress–strain data for aluminium alloy 7050-T74.*

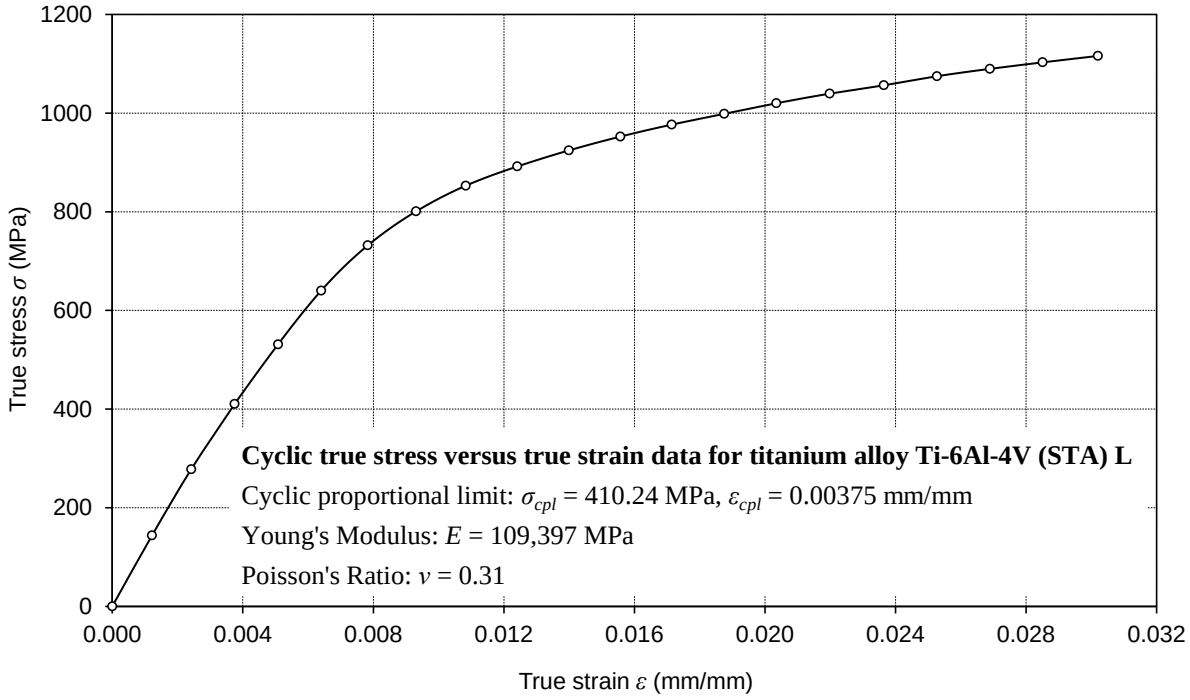

Figure 6: *Cyclic true stress–strain data for titanium alloy Ti-6Al-4V (STA) L.*

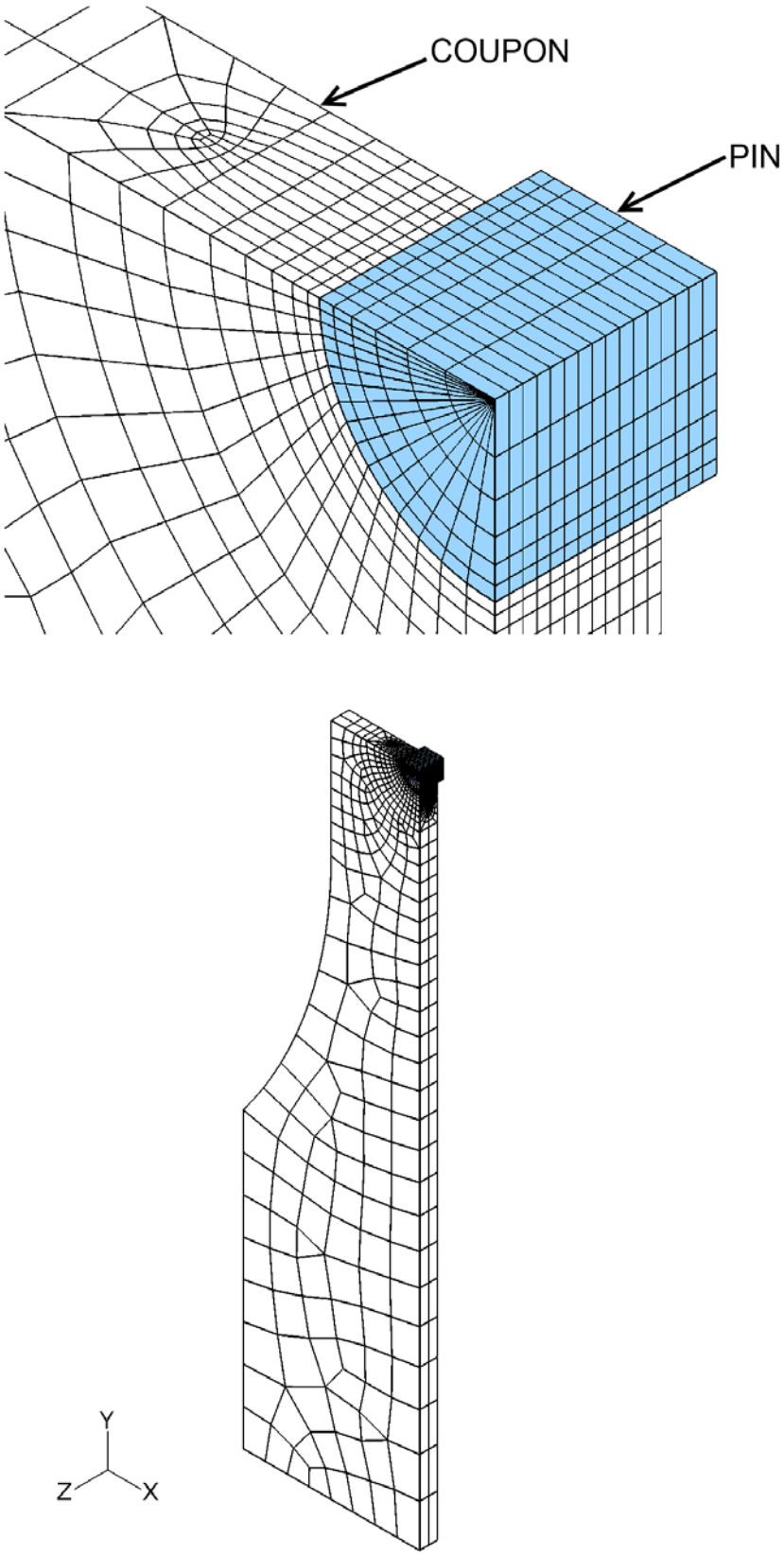

Figure 7: *Abaqus finite element mesh used to model the coupon and the pin for the linear-elastic contact analysis. Lower picture: complete ⅛-symmetry model. Upper picture: detail of finite element mesh in the vicinity of hole in the coupon, including the pin.*

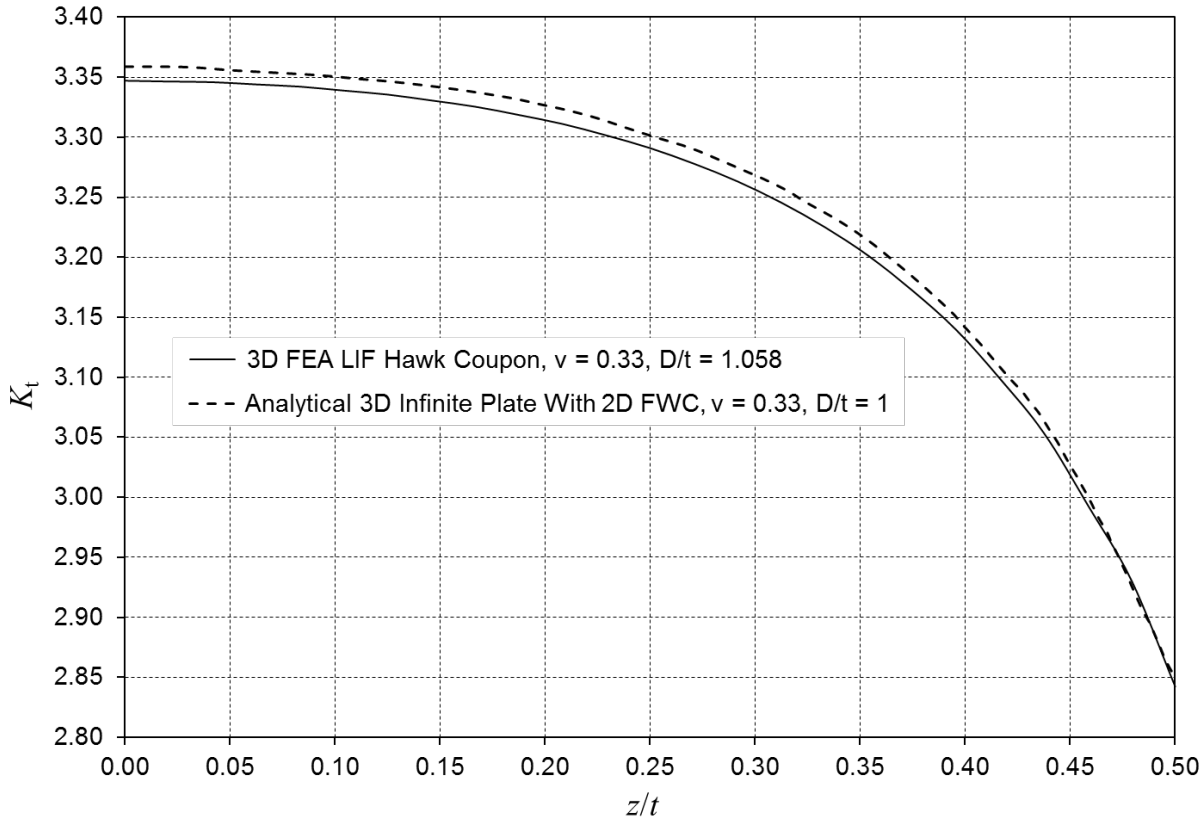

Figure 8: *Stress concentration factor along the bore of the hole for the aluminium coupon with an empty hole with the coupon loaded in uniaxial tension. Results obtained from Abaqus 3D FEA and a 2D finite-width-corrected 3D analytical solution for an infinite plate.*

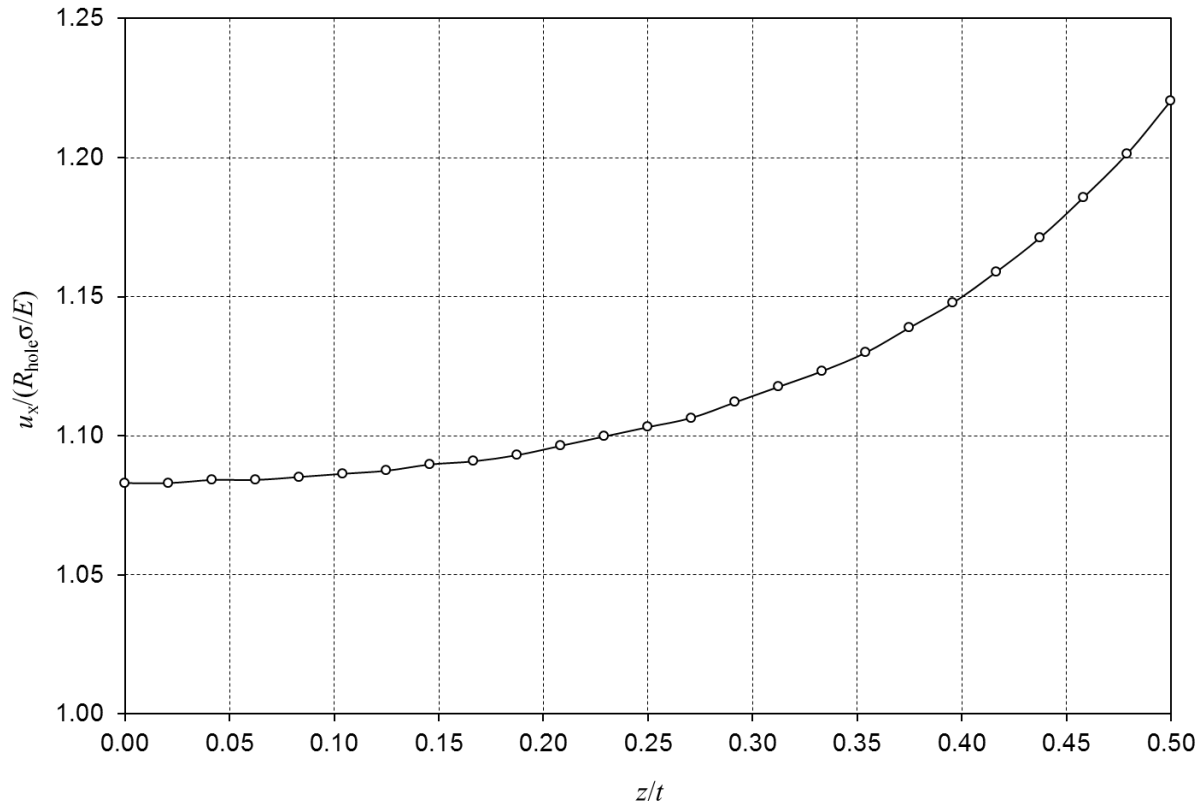

Figure 9: *Linear-elastic nondimensional transverse displacement of the hole edge in the thickness direction for the coupon loaded in uniaxial tension.*

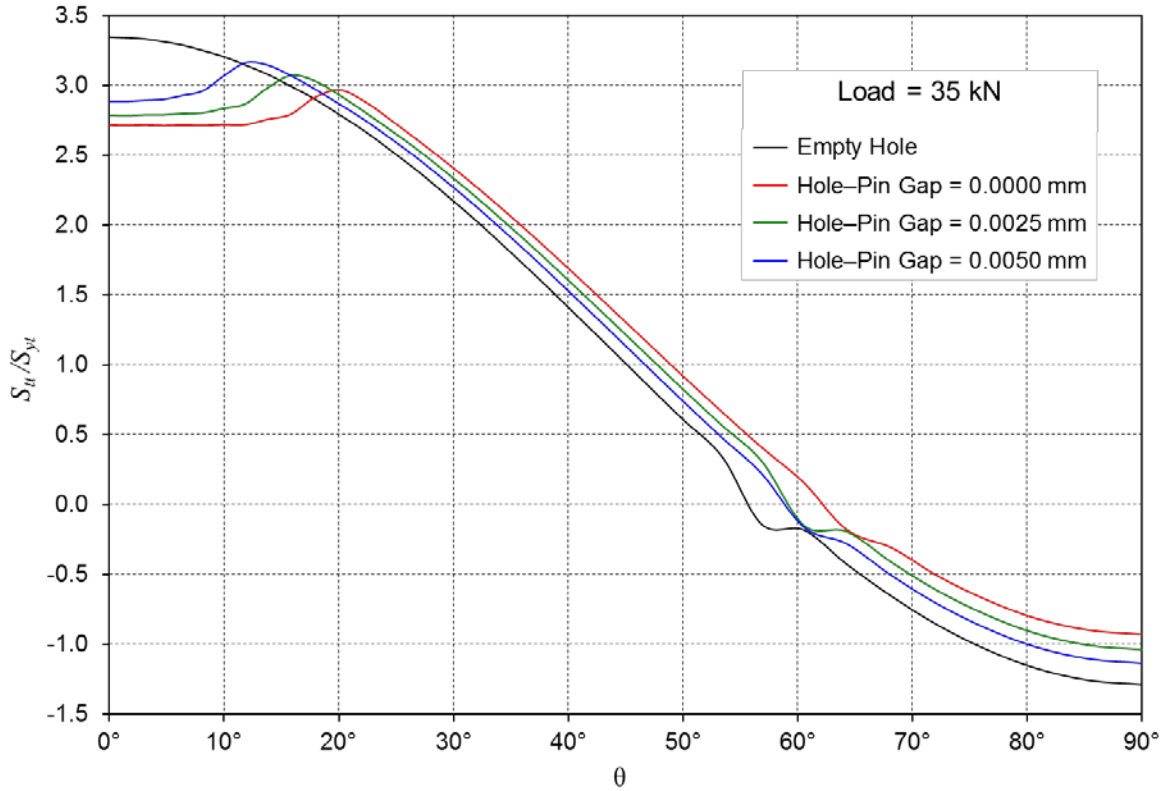

Figure 10: *Linear-elastic 3D FEA angular distributions of the normalised tangential stress around the hole edge at the midplane of the plate for initial hole–pin gaps of 0 mm, 0.0025 mm, and 0.0050 mm, for a tension load level of 35 kN, as well as the empty-hole case.*

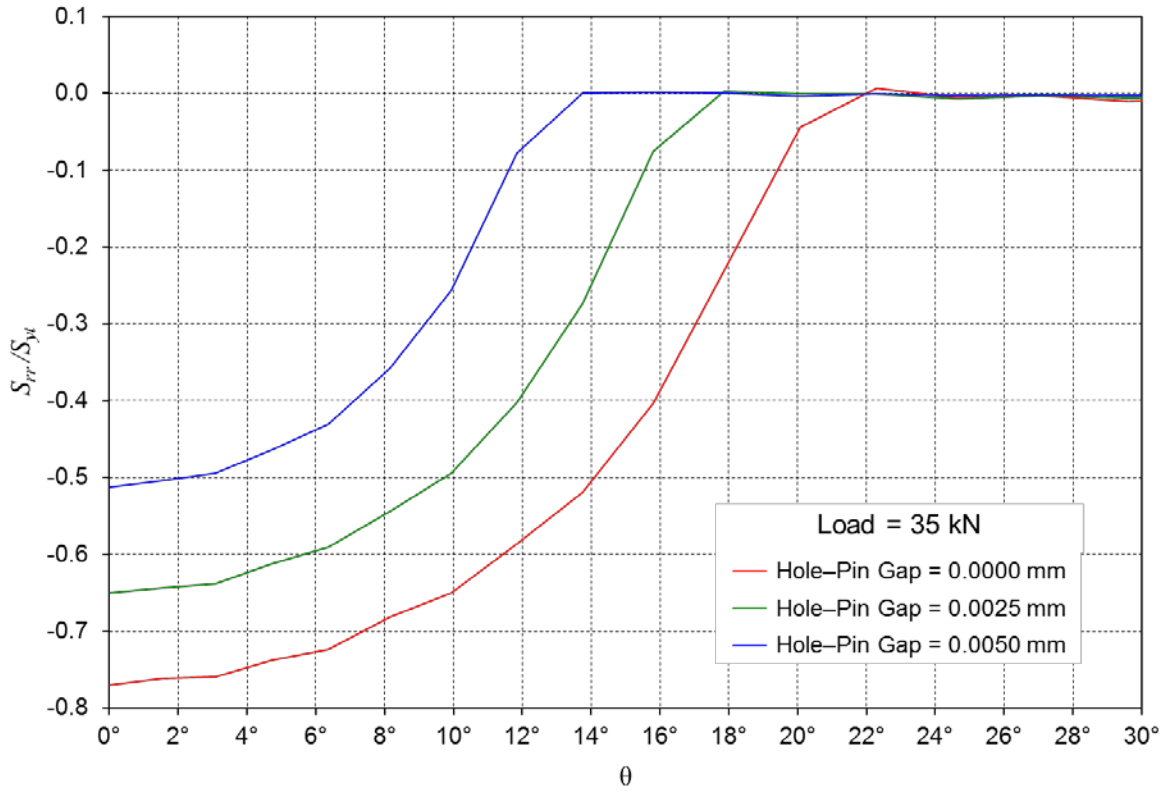

Figure 11: *Linear-elastic 3D FEA angular distributions of the normalised radial stress around the hole edge at the midplane of the plate for initial hole–pin gaps of 0 mm, 0.0025 mm, and 0.0050 mm, for a tension load level of 35 kN.*

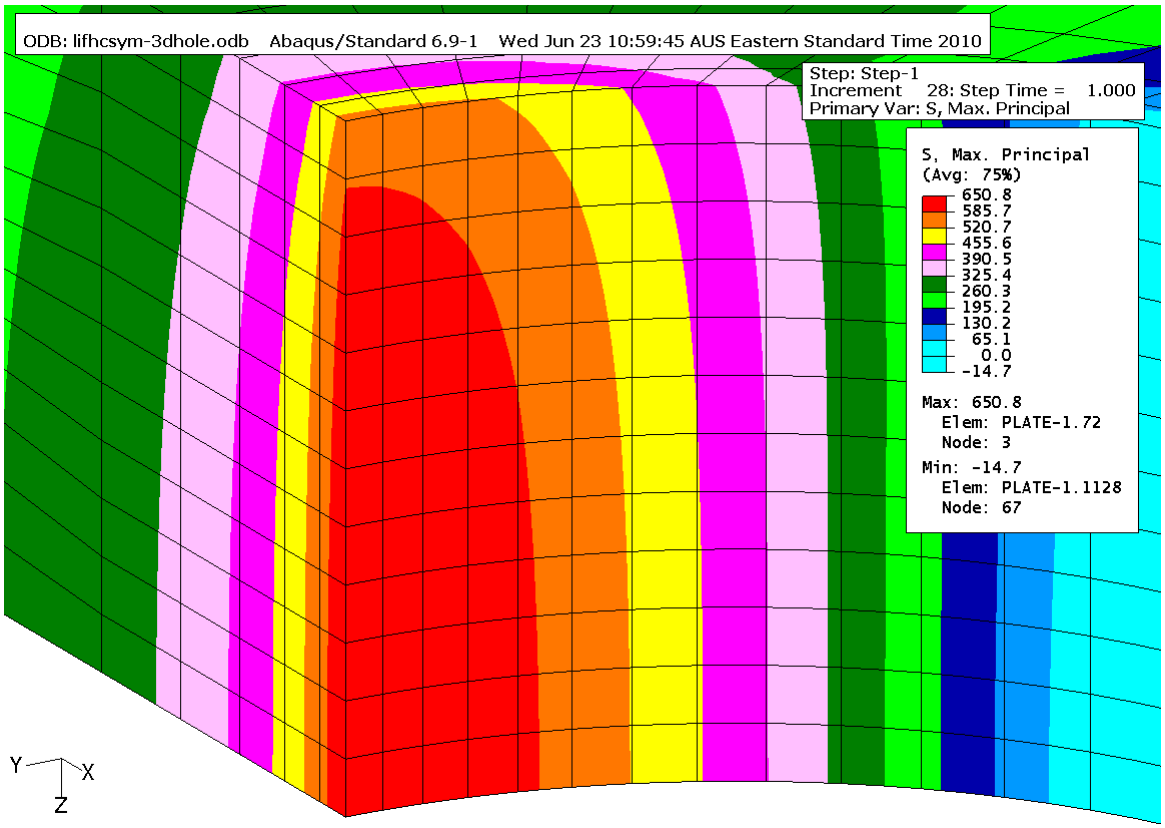

Figure 12: *Linear-elastic contour plot of maximum principal stress field for the coupon with an empty hole at 35 kN remote load.*

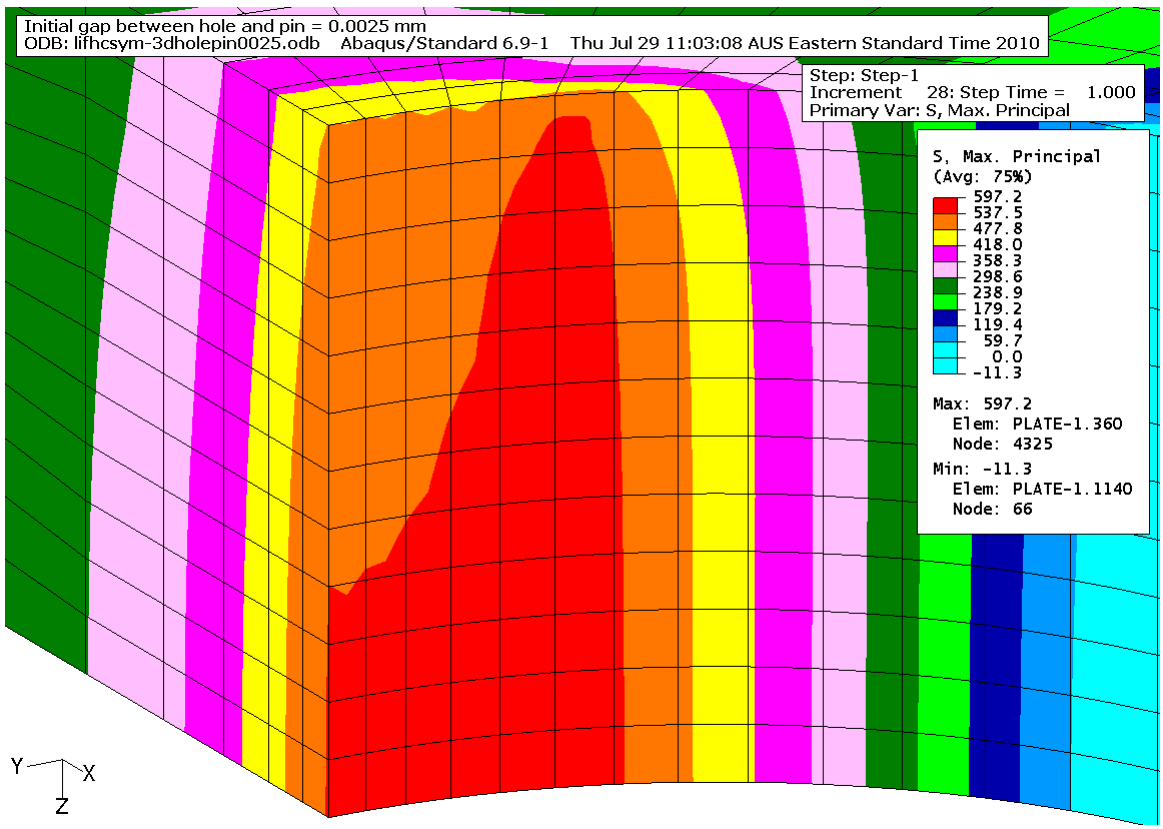

Figure 13: *Linear-elastic contour plot of maximum principal stress field for coupon with pin inserted for an initial gap of 0.0025 mm (diametric clearance of 0.0050 mm) at 35 kN remote load.*

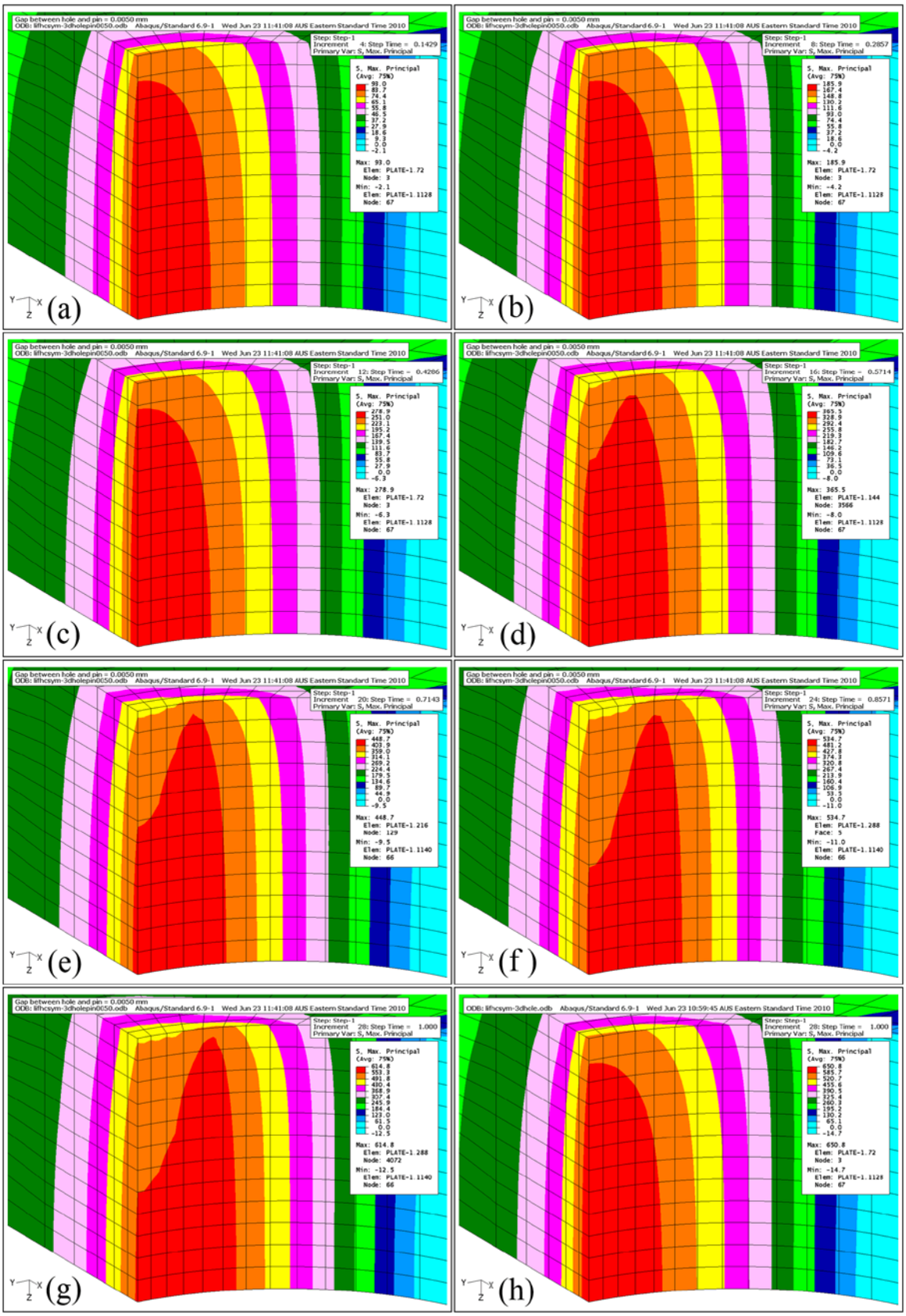

Figure 14: *Linear-elastic contour plots of maximum principal stress field for coupon hole–pin initial gap of 0.0025 mm (diametric clearance of 0.0050 mm), as well as the empty-hole case . (a)–(g) Coupon with hole and pin for remote load levels of 5 kN, 10 kN, 15 kN, 20 kN, 25 kN, 30 kN, and 35 kN, respectively. (h) Coupon with empty hole at 35 kN remote load.*

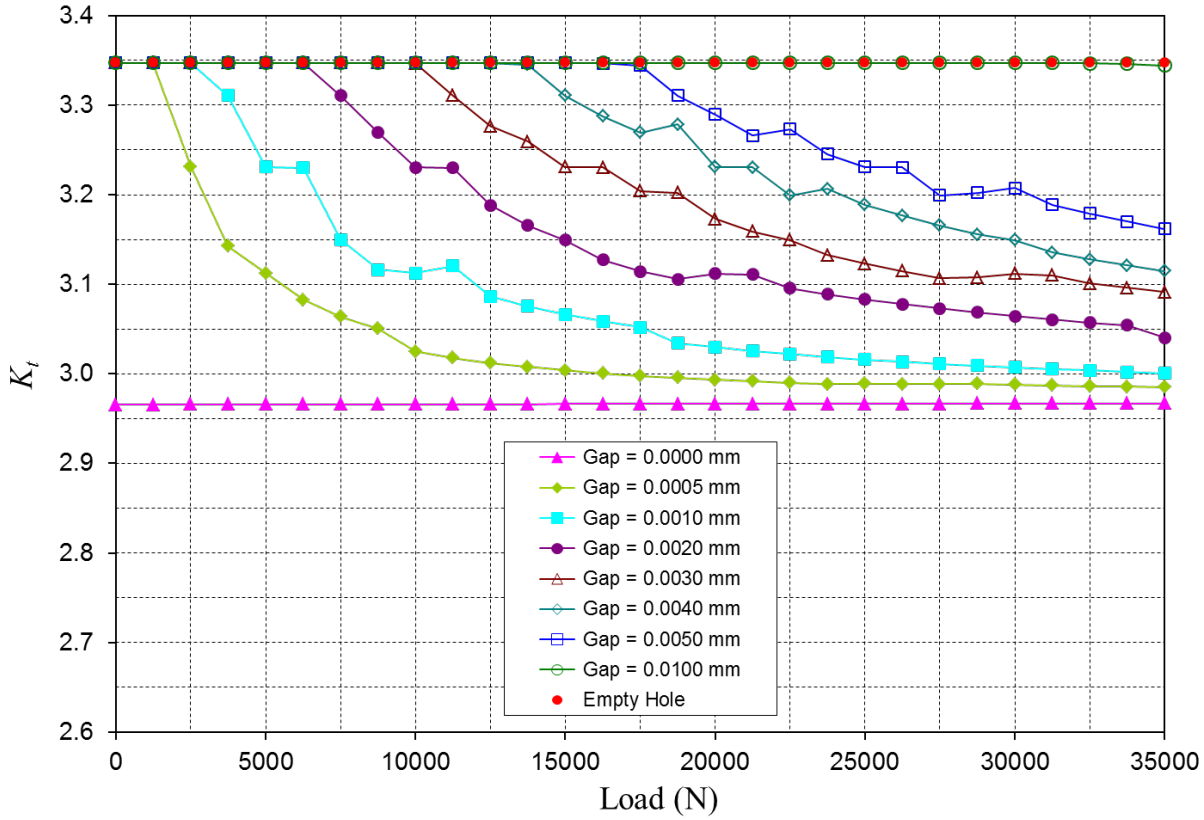

Figure 15: *Linear-elastic maximum* K_t *for the hole in the coupon as a function of load for a variety of hole–pin gaps, as well as for the empty-hole case.*

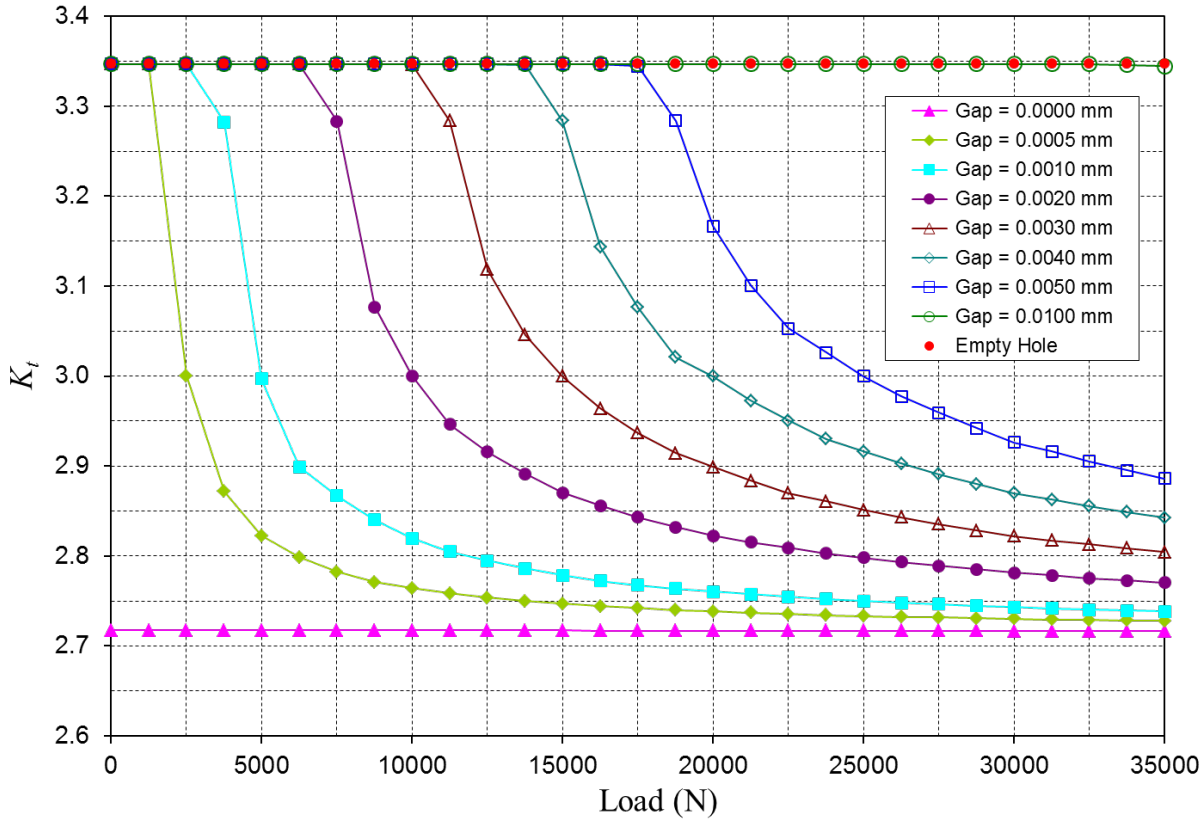

Figure 16: *Linear-elastic* K_t *for the hole in the coupon at the* $\theta = 0°$ *location on the hole boundary as a function of load for a variety of hole–pin gaps, as well as for the empty-hole case.*

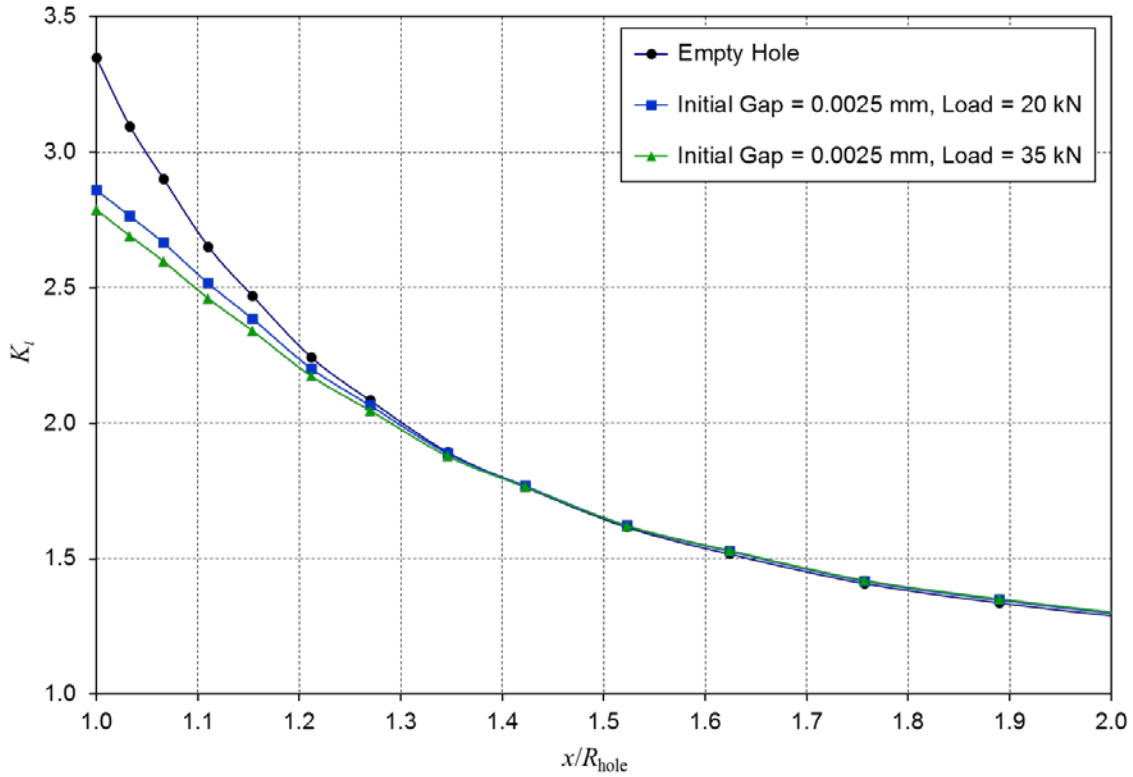

Figure 17: *Linear-elastic stress decay as a function of radial distance away from the edge of the hole at the θ = 0° location for an initial gap of 0.0025 mm (diametric clearance of 0.0050 mm) and the empty-hole case, as represented by* K_t *based on the maximum principal stress.*

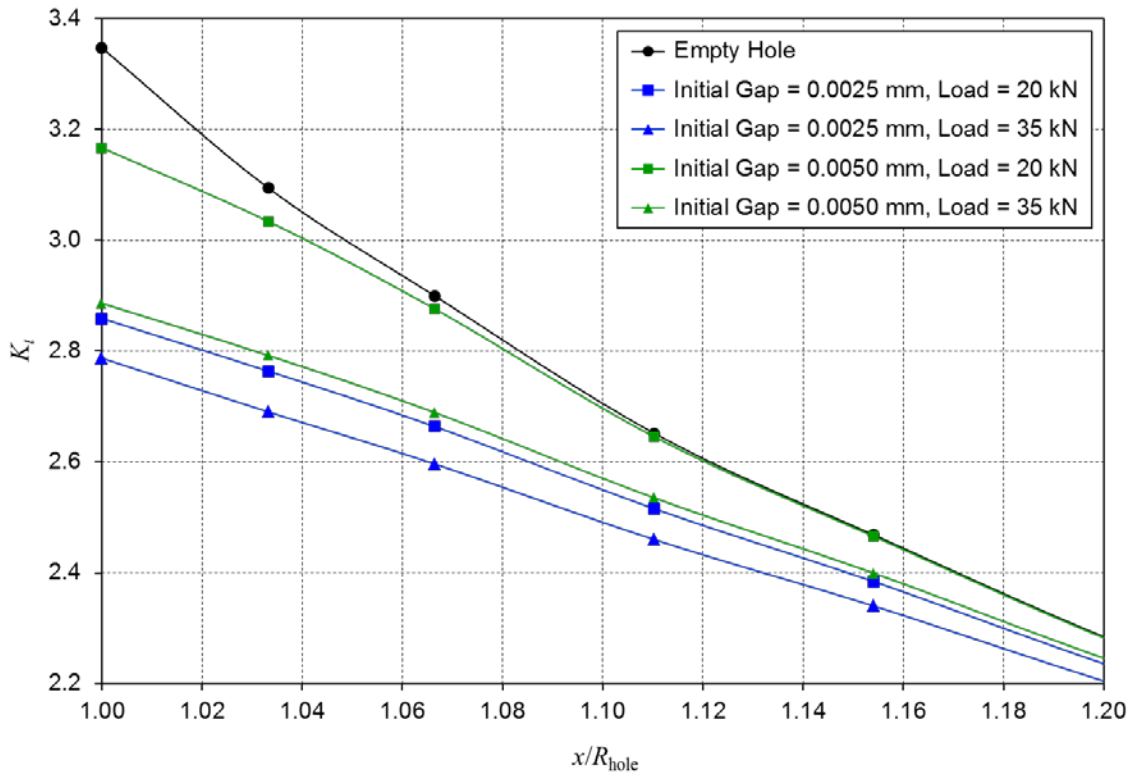

Figure 18: *Comparison of linear-elastic stress decay as a function of radial distance away from the edge of the hole at the θ = 0° location for two initial gaps of 0.0025 mm and 0.0050 mm (diametric clearances of 0.0050 mm and 0.0100 mm), and the empty-hole case, as represented by* K_t *based on the maximum principal stress.*

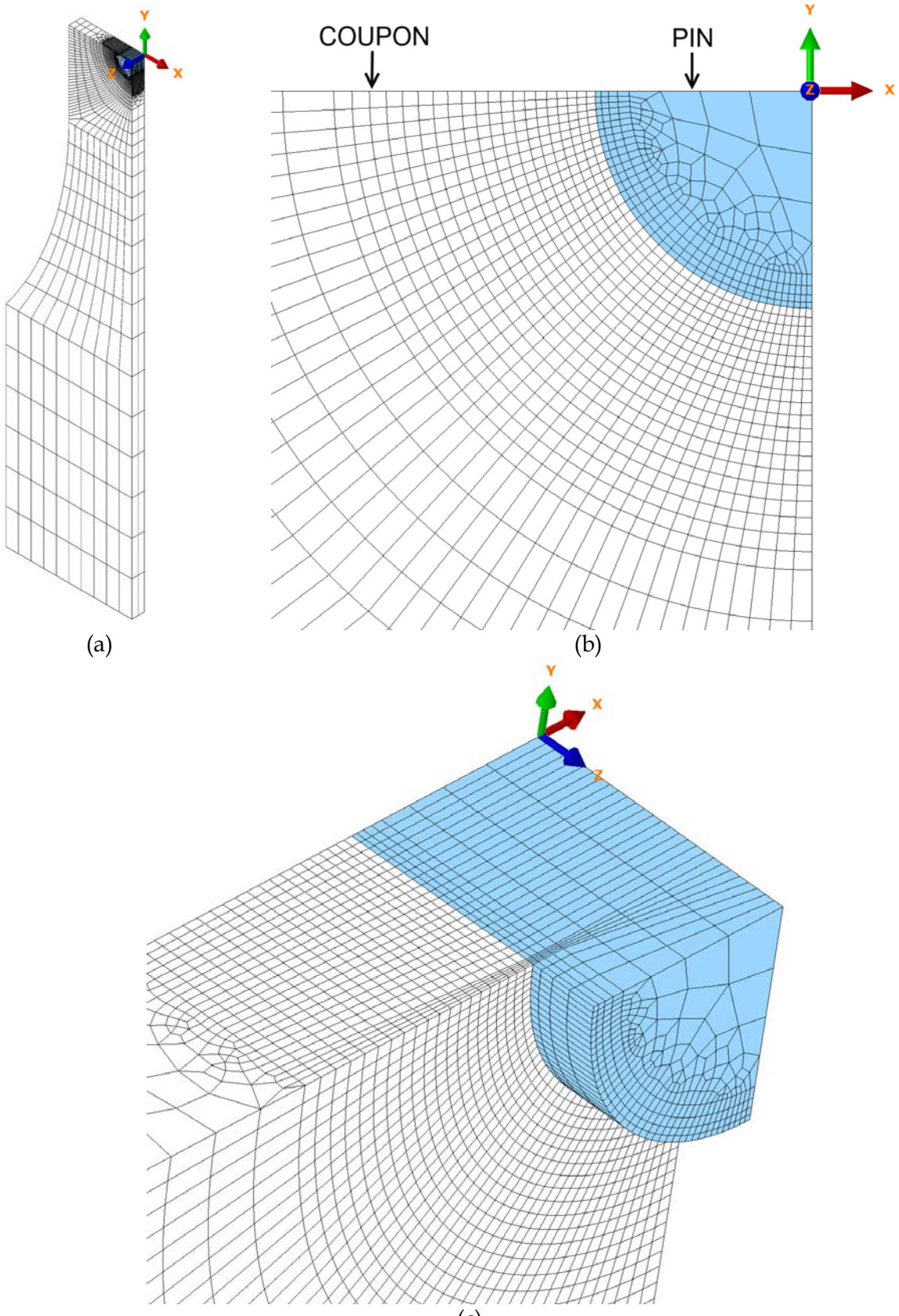

Figure 19: *Abaqus graded-mesh 3D finite element model of the aluminium coupon and the neat-fit titanium pin. (a) Complete ⅛-symmetry model. (b) Side-on view of plate and pin mesh showing grading around hole–pin boundary. (c) Detail of mesh in vicinity of hole–pin interface.*

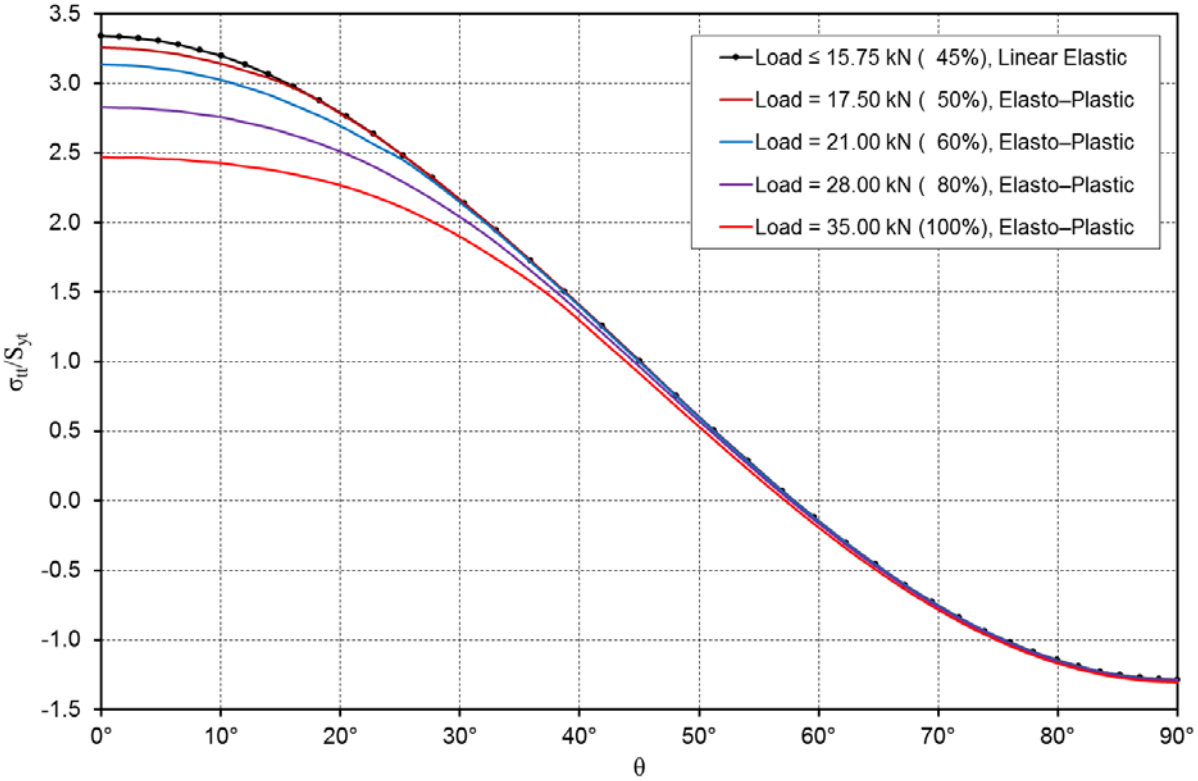

Figure 20: *Normalised tangential stress around the boundary of the hole at the midplane of the plate for the empty-hole case and a range of tension load levels, corresponding to linear-elastic and elasto–plastic response regimes.*

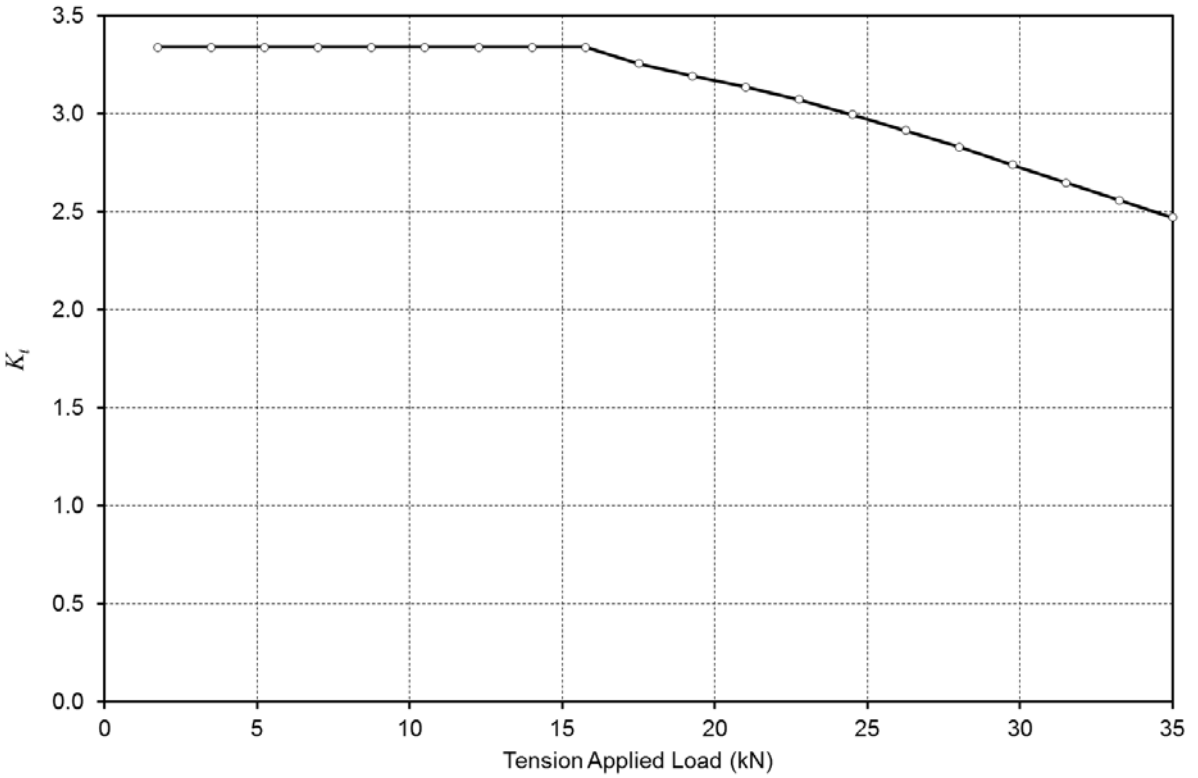

Figure 21: *Variation in* K_t *for the empty-hole case as a function of applied tension load for linear-elastic and elasto–plastic response regimes.*

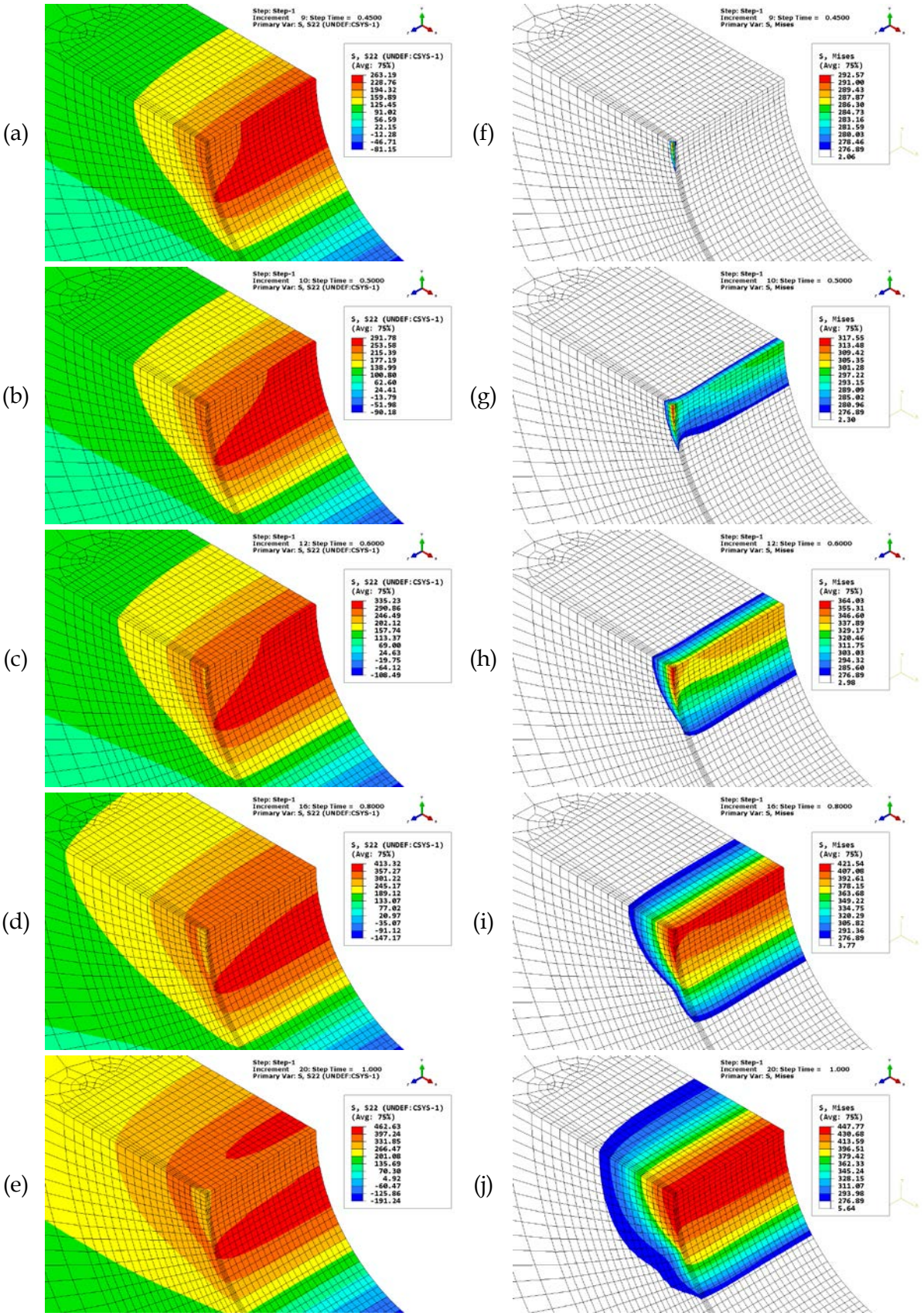

Figure 22: *Stress contours for the hole during hole–pin contact, corresponding to increasing remote uniaxial tension load levels of 15.75 kN, 17.5 kN, 21.0 kN, 28.0 kN, and 35.0 kN. (a)–(e) Elasto–plastic tangential stress. (f)–(j) Plastic-zone von Mises stress (proportional limit is* σ_{cpl} *= 276.9 MPa).*

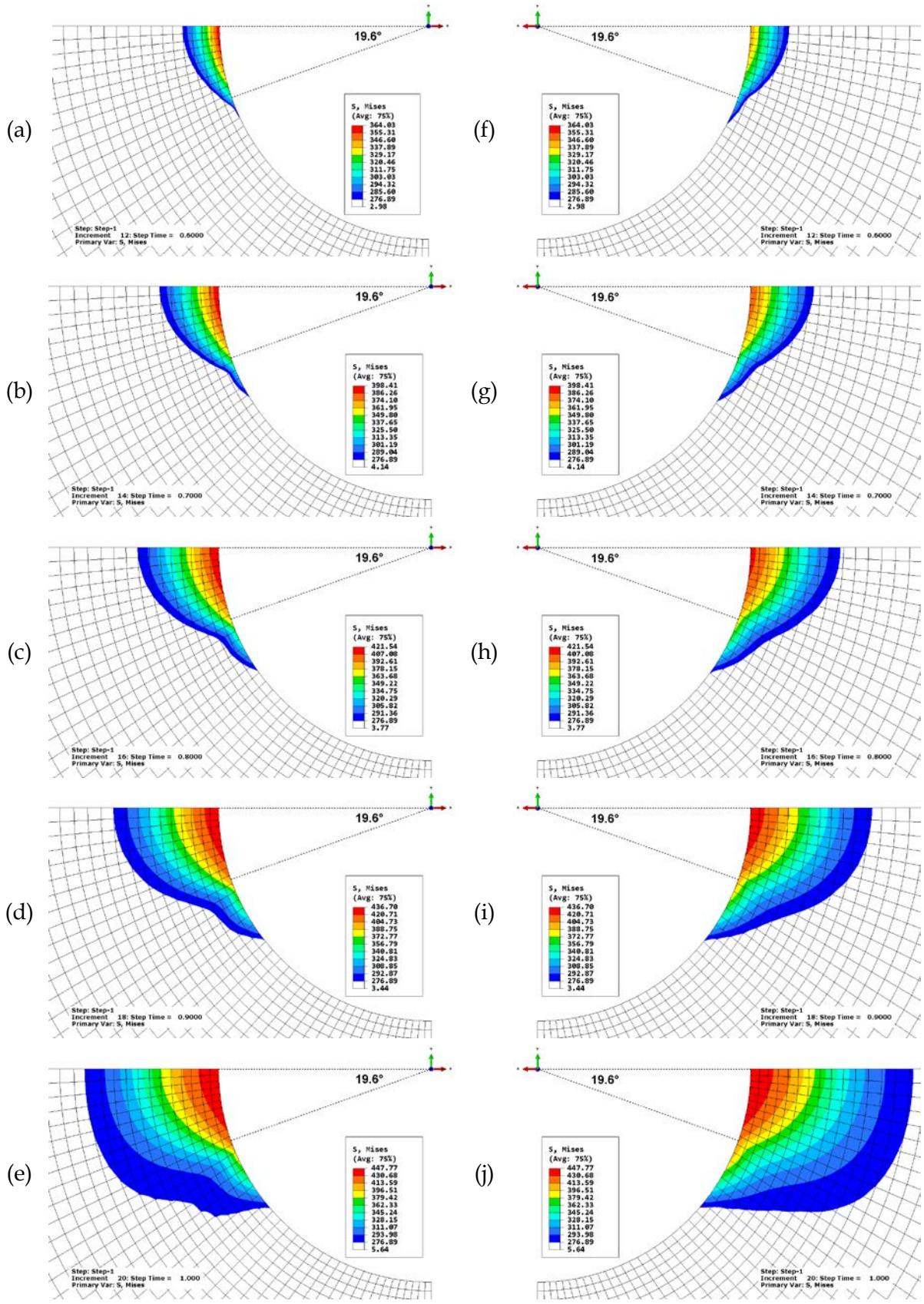

Figure 23: *Plastic-zone von Mises stress contours for the hole during hole–pin contact, corresponding to increasing remote uniaxial tension load levels of 21.0 kN, 24.5 kN, 28.0 kN, 31.5 kN, and 35.0 kN (proportional limit is* σ_{cpl} *= 276.89 MPa). (a)–(e) Stress at free surface. (f)–(j) Stress at midplane surface.*

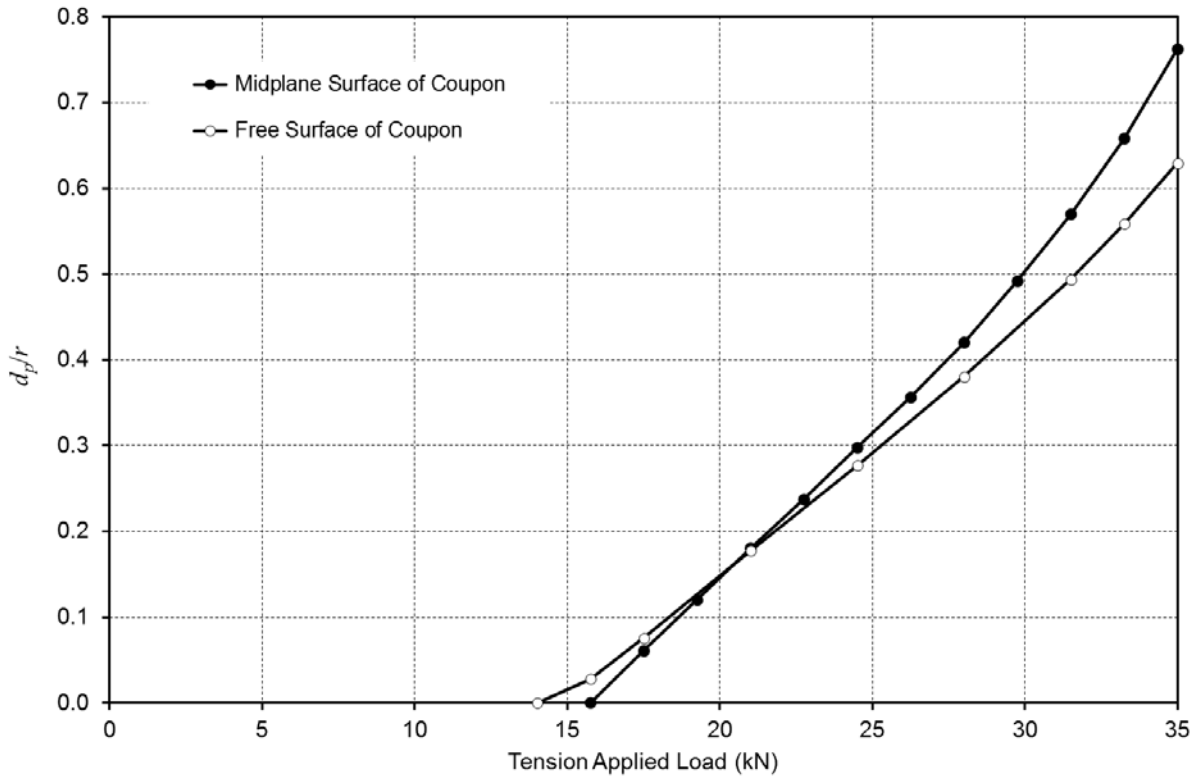

Figure 24: *Variation in the normalised depth of the plastic zone,* d_p/r*, along the* x*-axis as a function of tension applied load for the neat-fit filled-hole case.*

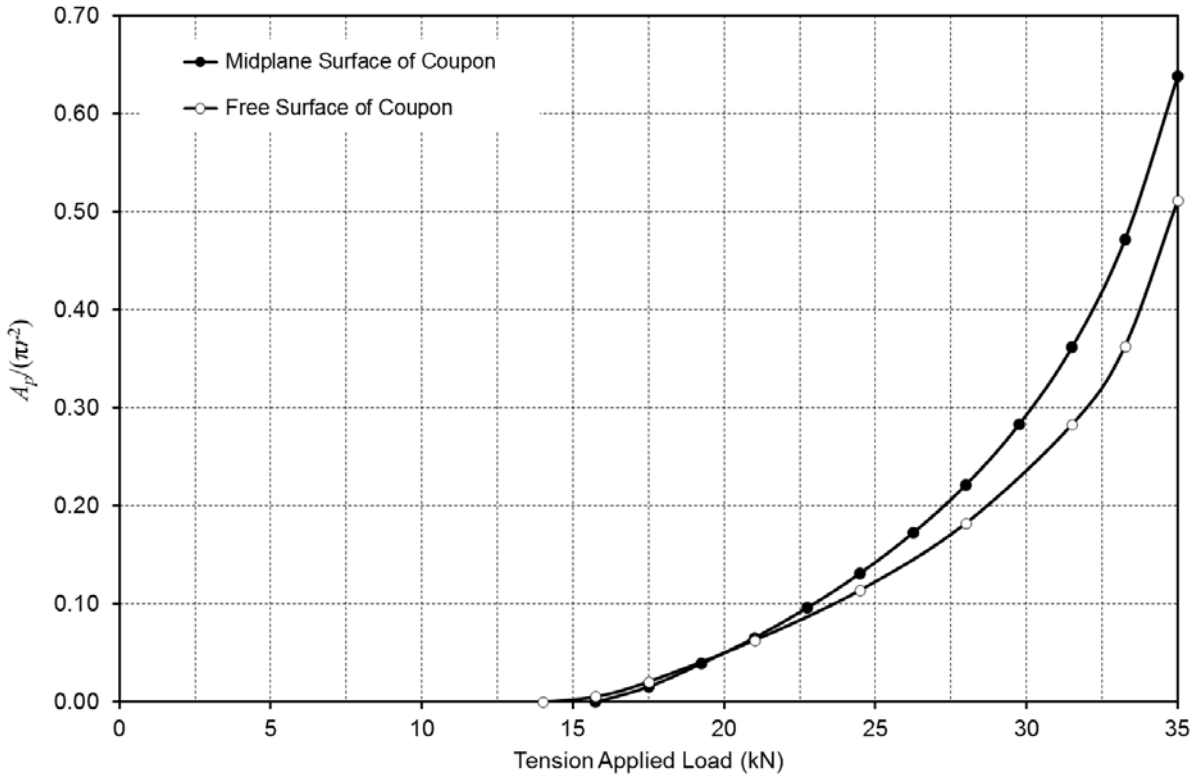

Figure 25: *Variation in the normalised area of the plastic zones,* $A_p/(\pi r^2)$*, as a function of tension applied load for the neat-fit filled-hole case.*

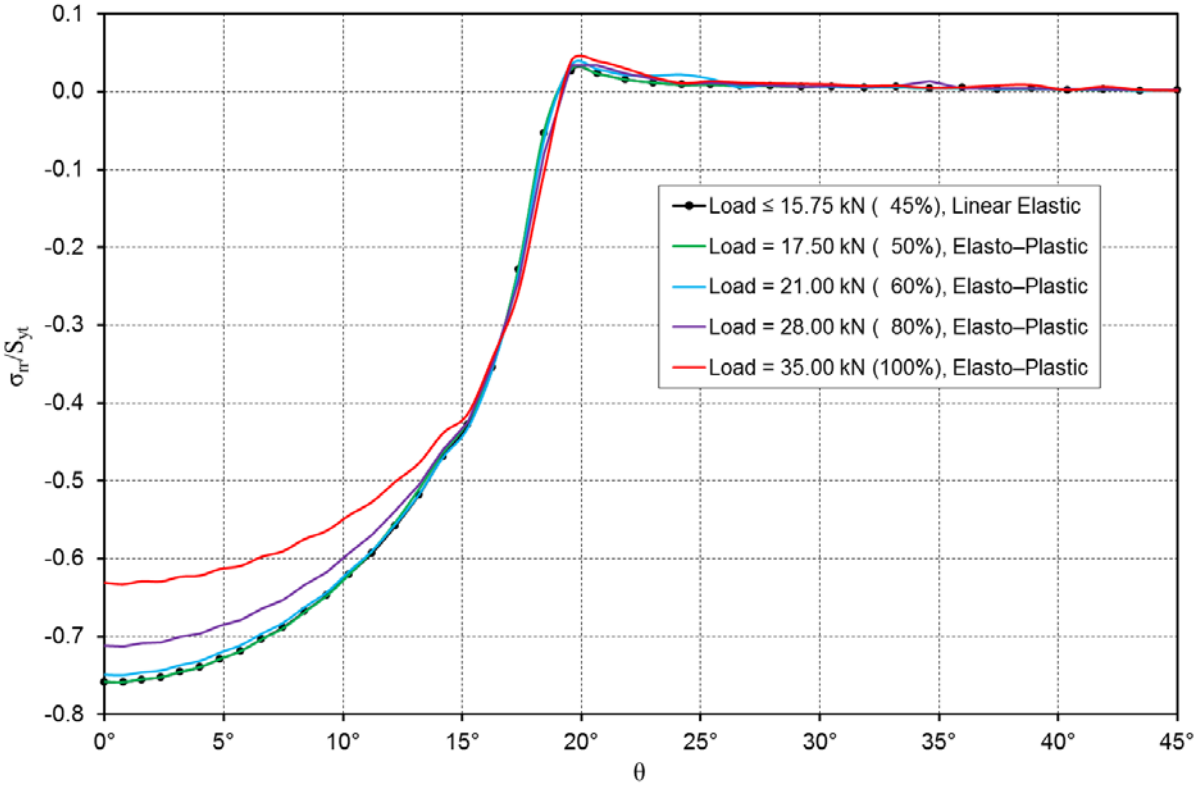

Figure 26: *Normalised radial stress around the boundary of the hole at the midplane of the plate for the neat-fit filled-hole case and a range of tension load levels, corresponding to linear-elastic and elasto–plastic response regimes.*

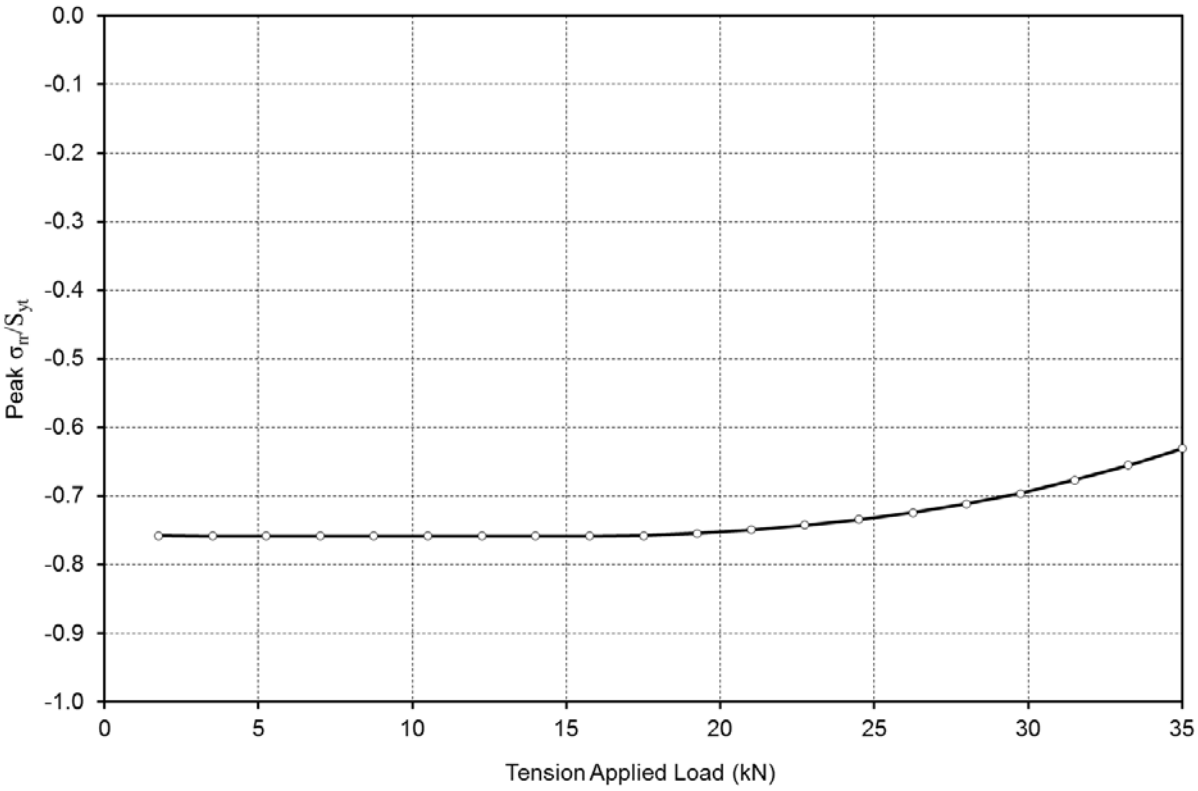

Figure 27: *Normalised peak radial stress around the boundary of the hole at the midplane of the plate for the neat-fit filled-hole case and a range of tension load levels.*

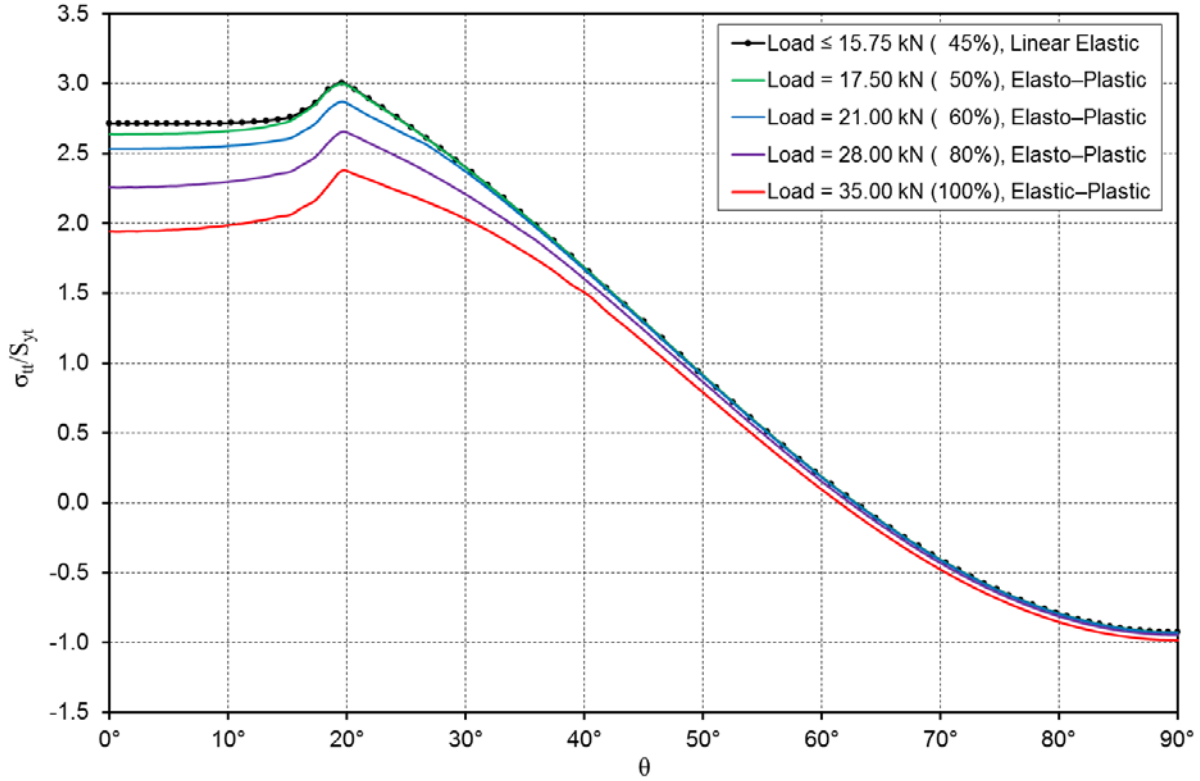

Figure 28: *Normalised tangential stress around the boundary of the hole at the midplane of the plate for the neat-fit filled-hole case and a range of tension load levels, corresponding to linear-elastic and elasto–plastic response regimes.*

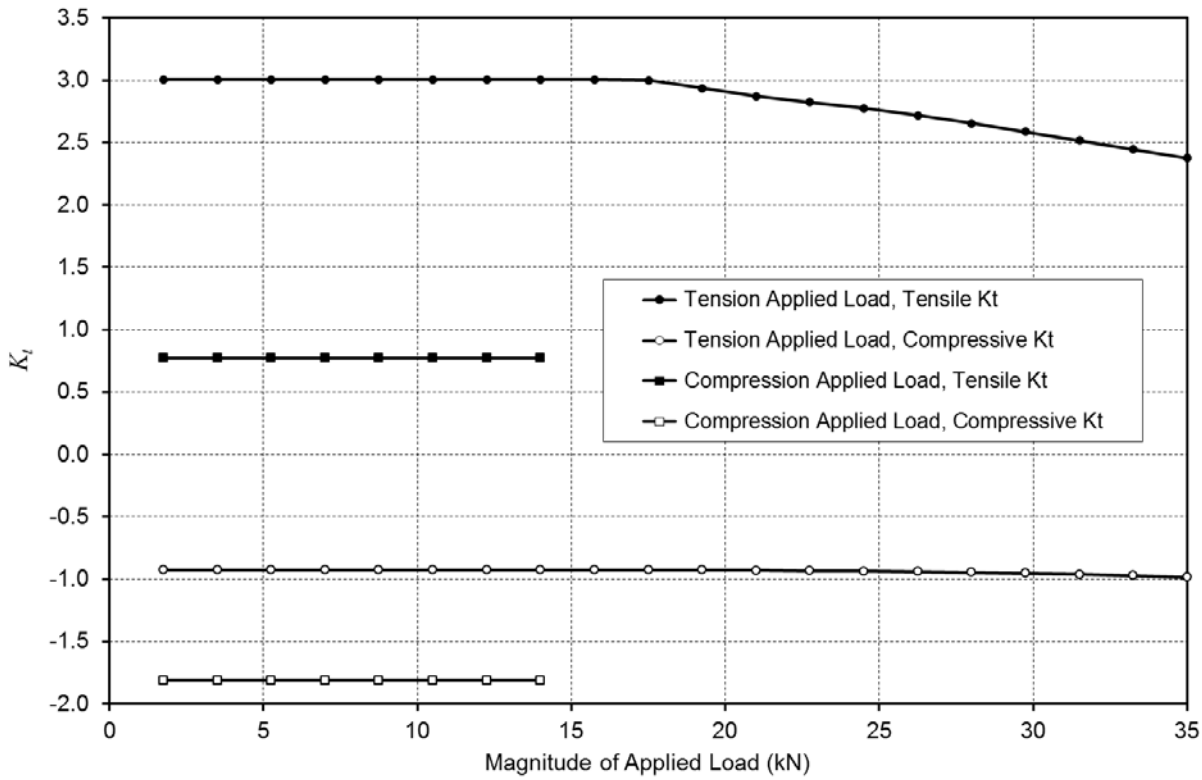

Figure 29: *Variation of tensile and compressive values of peak* K_t *at the midplane of the plate with increasing magnitude of applied tension and compression load levels.*

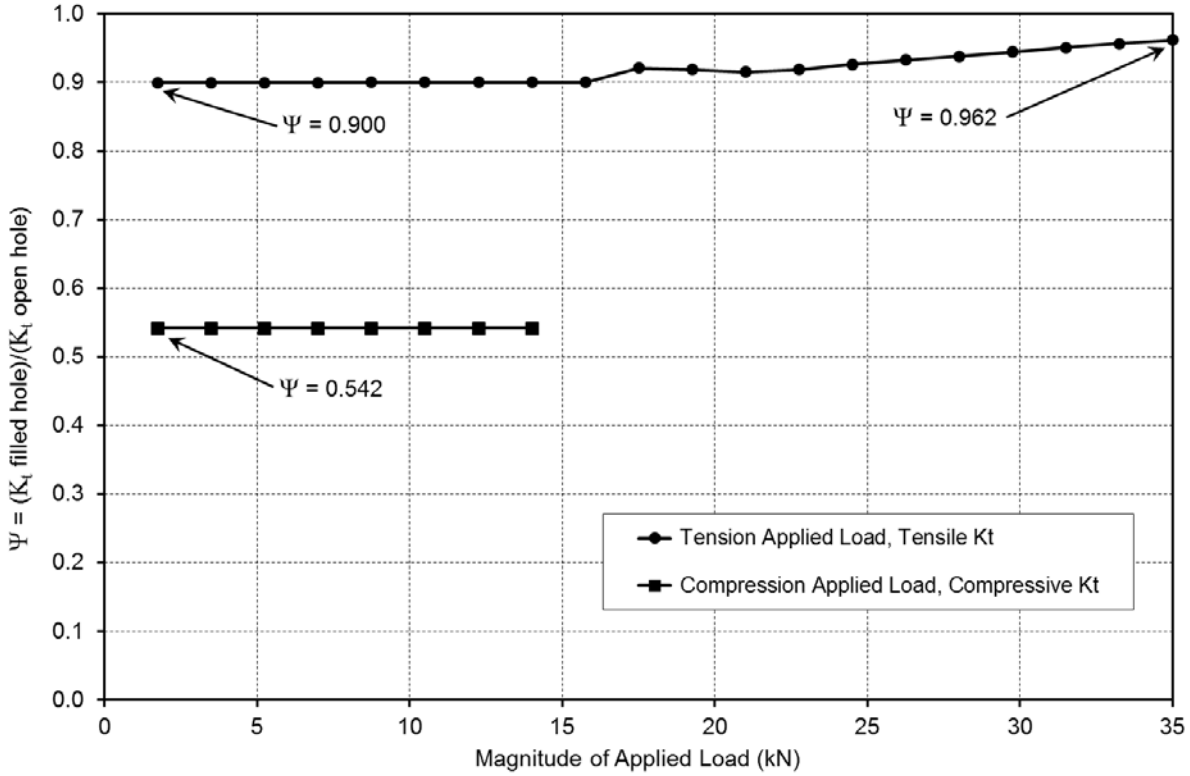

Figure 30: *Ratio of midplane K_t values obtained for the neat-fit filled-hole and the empty-hole cases, Ψ, as a function of applied remote load level in tension and compression.*

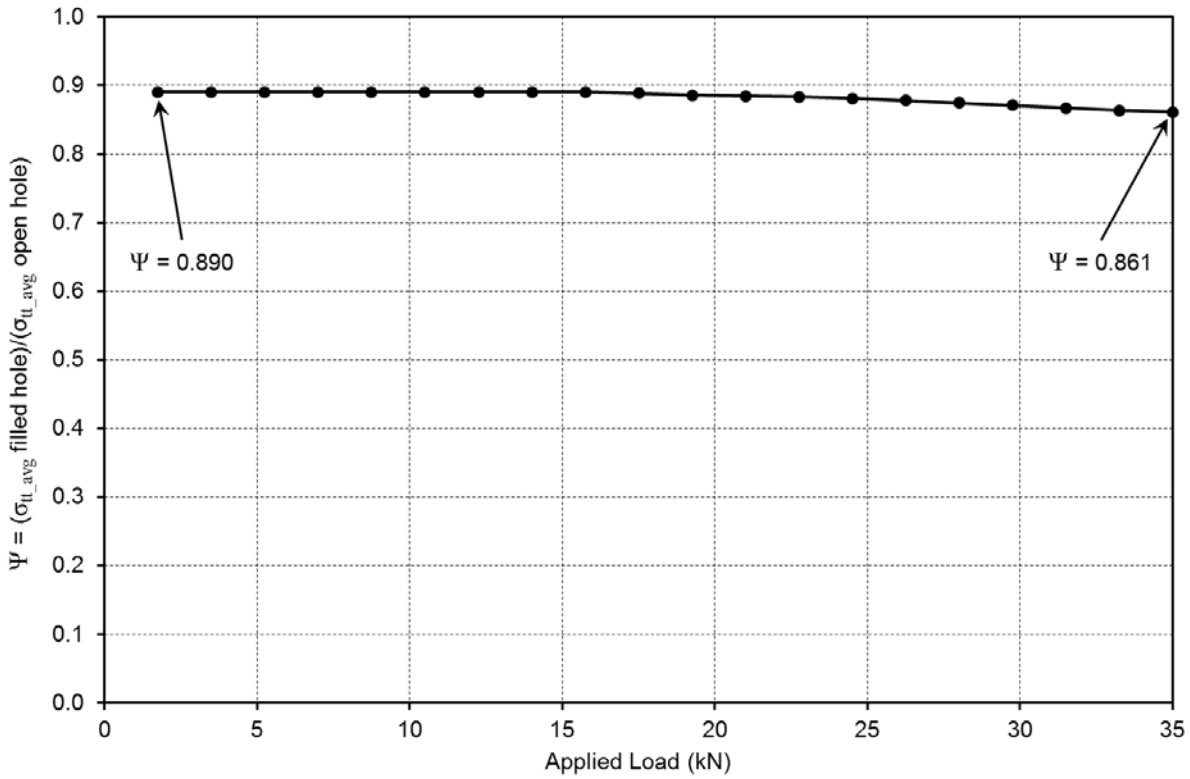

Figure 31: *Ratio of midplane averaged σ_{tt} values obtained for the neat-fit filled-hole and the empty-hole cases, Ψ, as a function of applied remote load level in tension. Averaging was performed over an angular region approximately 10% greater than the contact zone.*

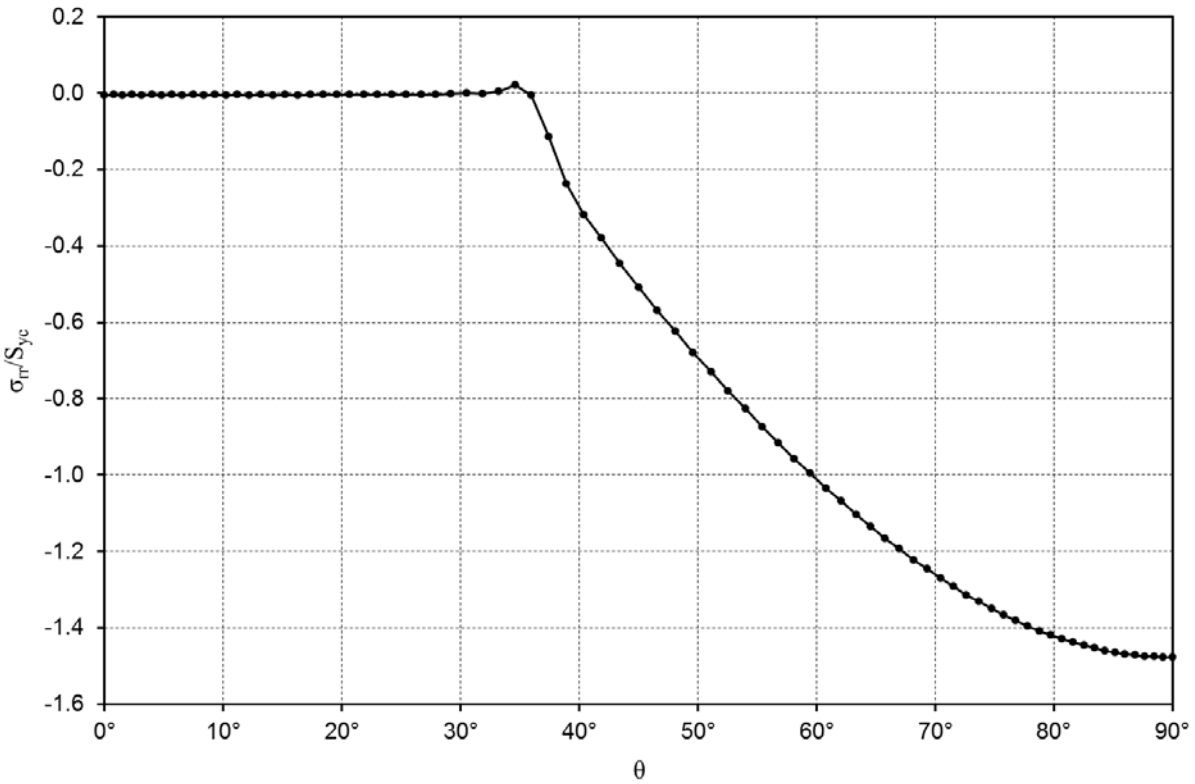

Figure 32: *Normalised radial stress around the boundary of the hole at the midplane of the plate for the neat-fit filled-hole case while undergoing compression loading.*

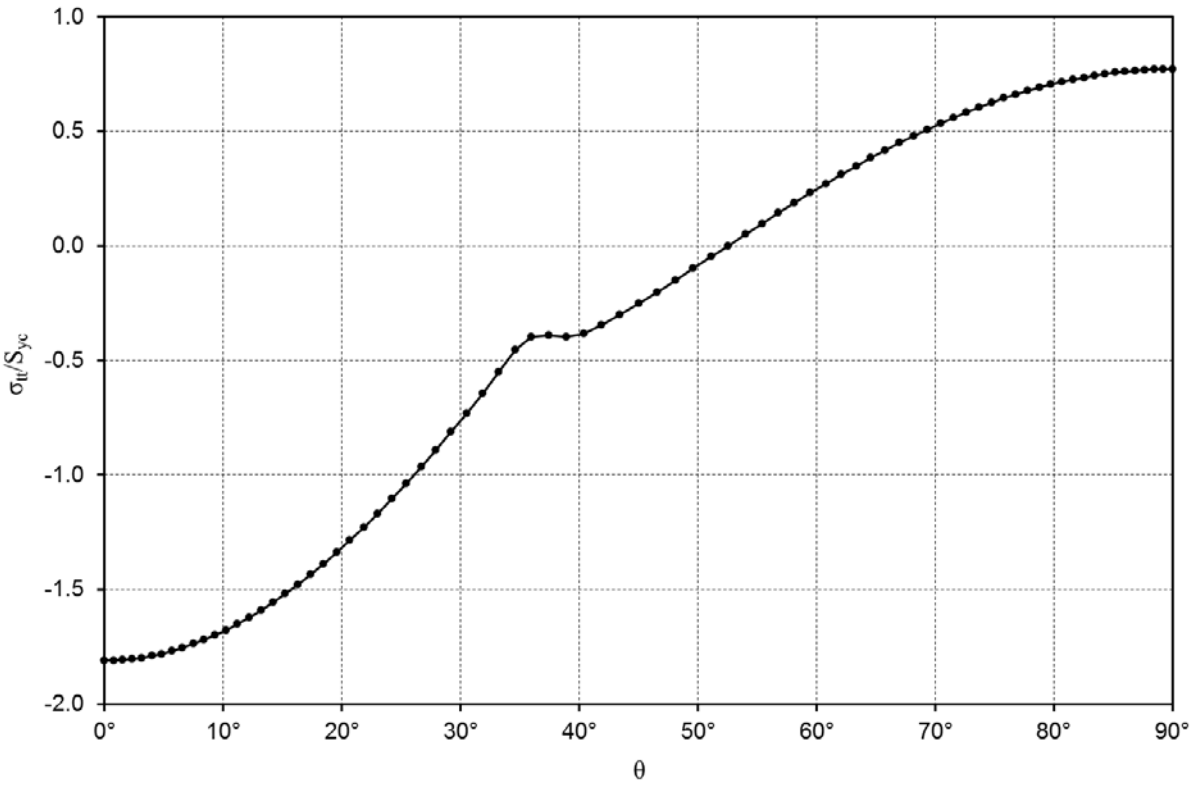

Figure 33: *Normalised tangential stress around the boundary of the hole at the midplane of the plate for the neat-fit filled-hole case while undergoing compression loading.*

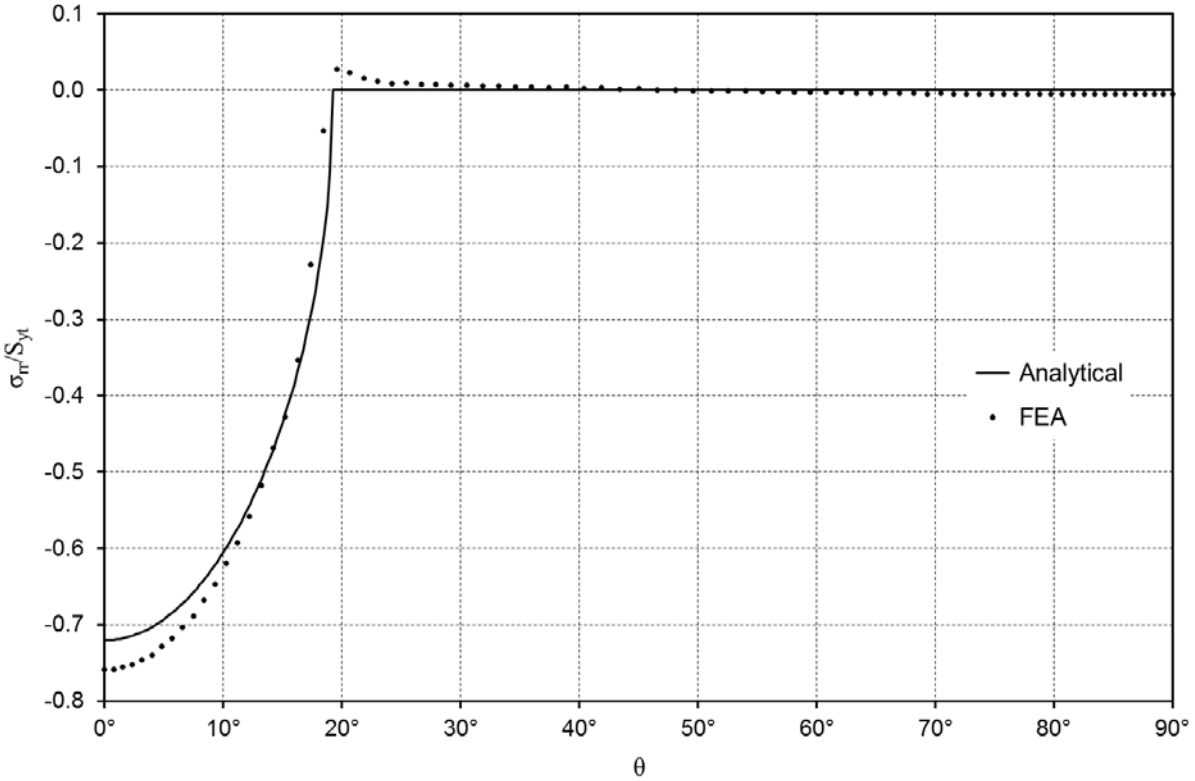

Figure 34: *Comparison of analytical and FEA predictions of the normalised radial stress around the boundary of the hole at the midplane of the plate for the neat-fit filled-hole case while undergoing tension loading in the linear-elastic response regime.*

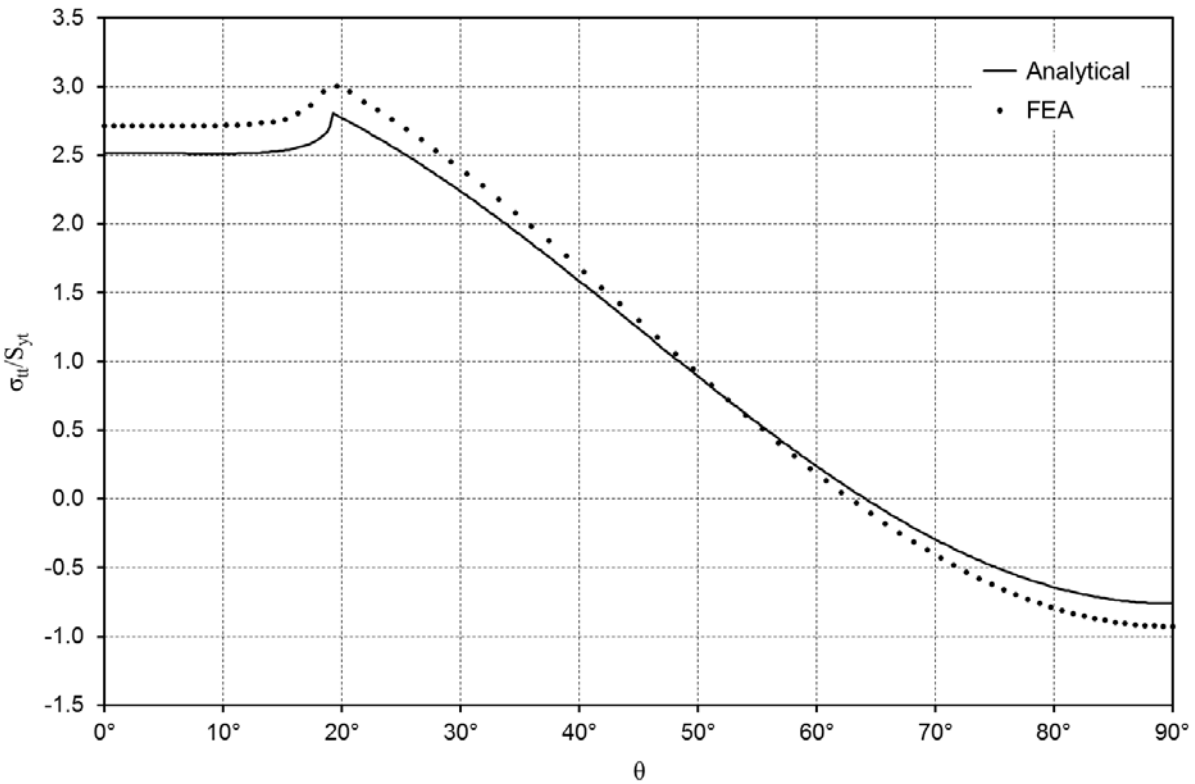

Figure 35: *Comparison of 2D analytical and 3D FEA predictions of the normalised tangential stress around the boundary of the hole at the midplane of the plate for the neat-fit filled-hole case while undergoing tension loading in the linear-elastic response regime.*

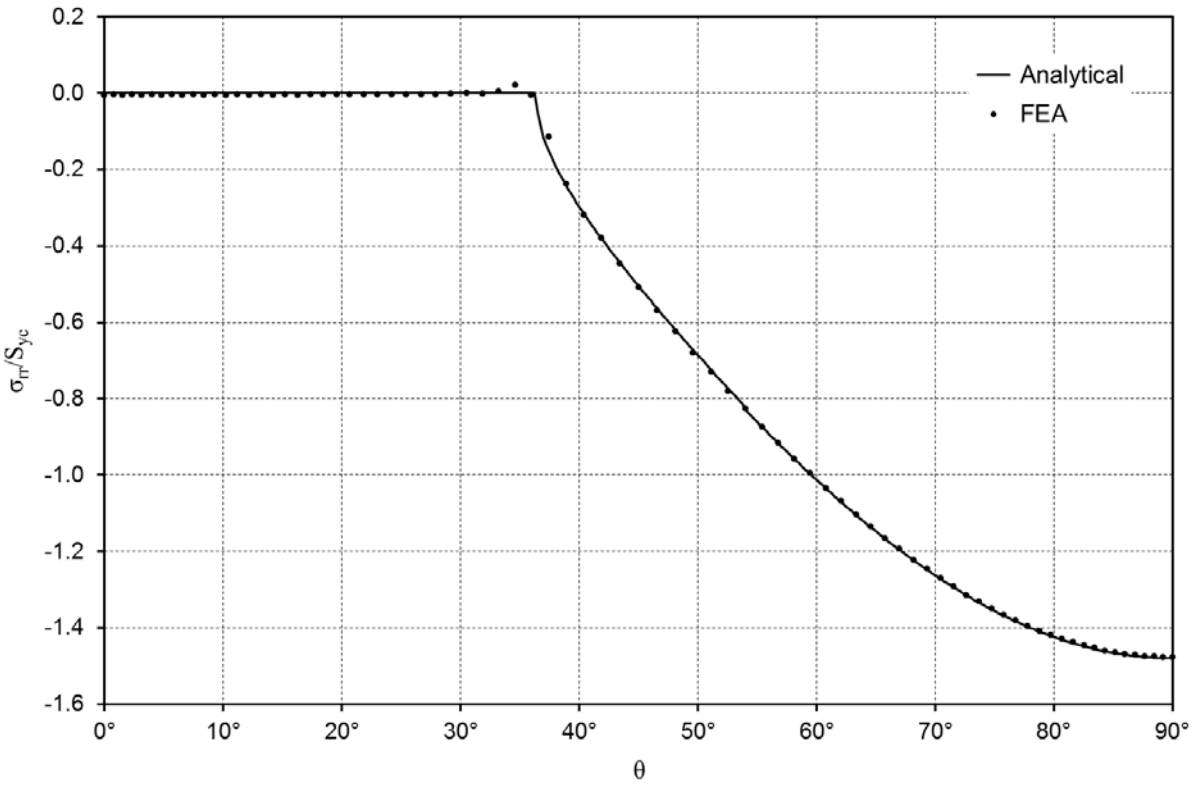

Figure 36: *Comparison of 2D analytical and 3D FEA predictions of the normalised radial stress around the boundary of the hole at the midplane of the plate for the neat-fit filled-hole case while undergoing compression loading in the linear-elastic response regime.*

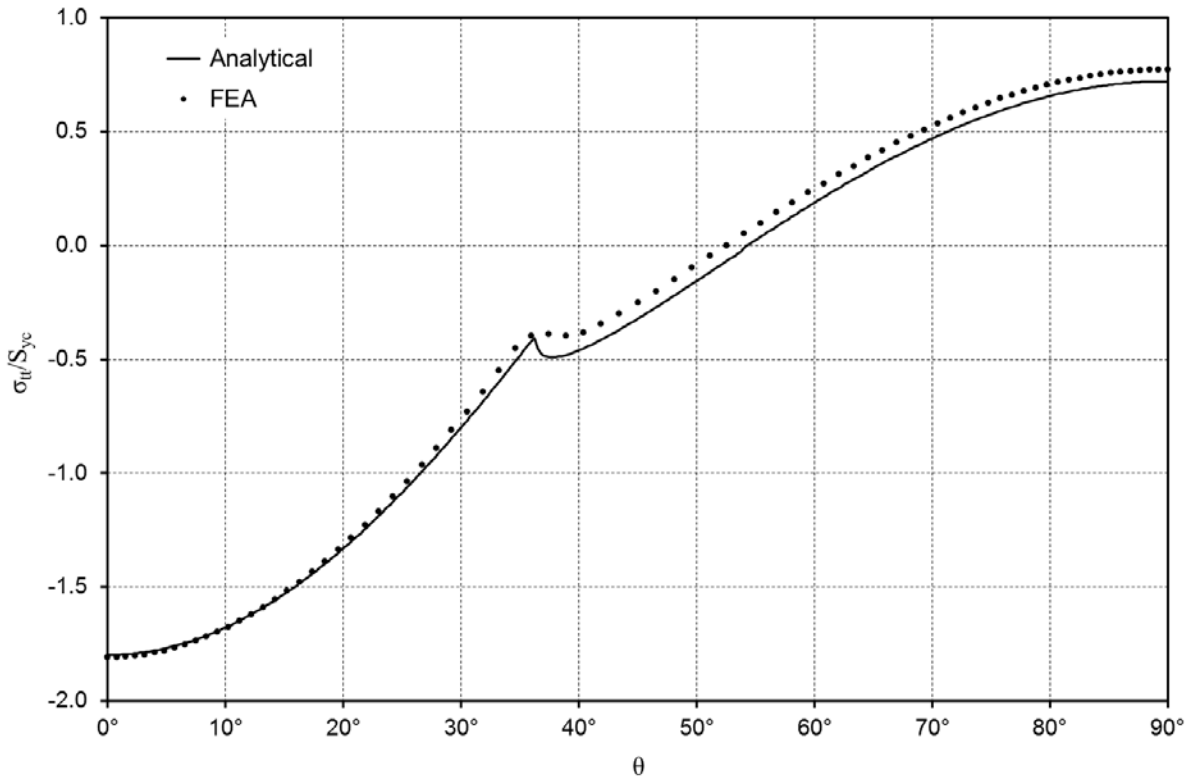

Figure 37: *Comparison of 2D analytical and 3D FEA predictions of the normalised tangential stress around the boundary of the hole at the midplane of the plate for the neat-fit filled-hole case while undergoing compression loading in the linear-elastic response regime.*

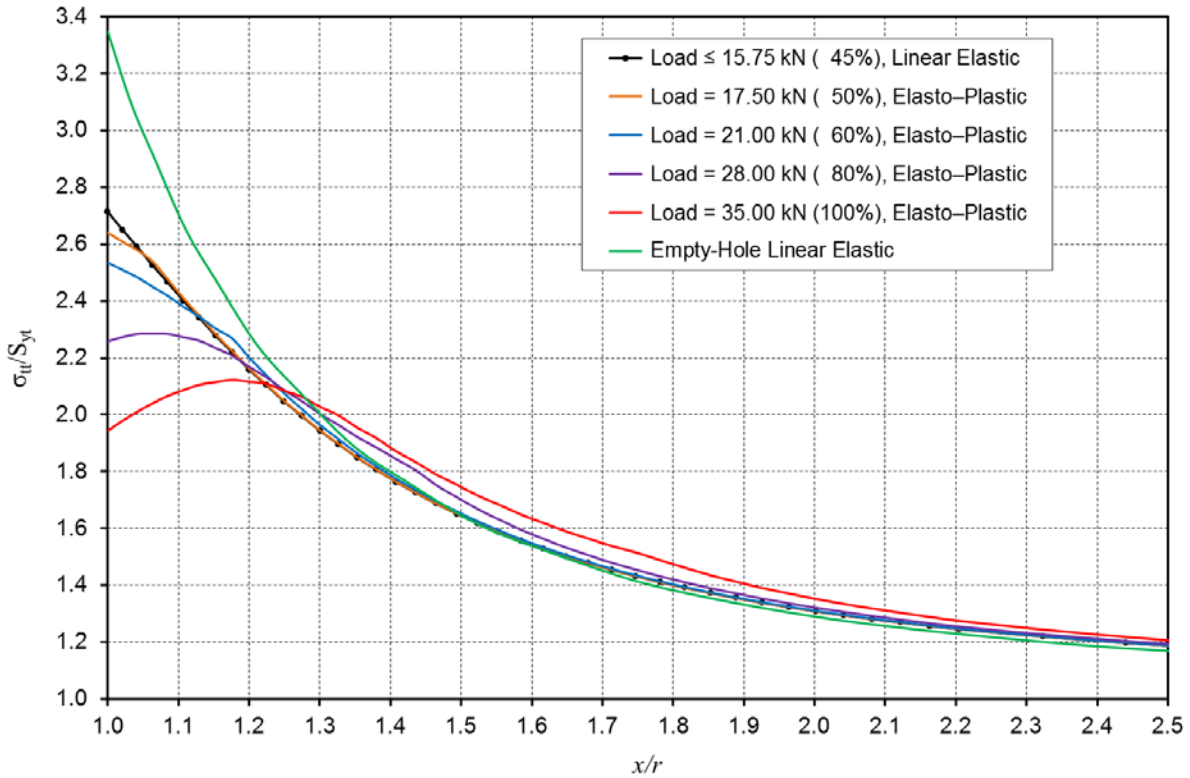

Figure 38: *Normalised tangential stress as a function of radial distance away from the edge of the hole at the θ = 0° location at midplane of plate, for the neat-fit filled-hole and empty-hole cases for a range of tension load levels, corresponding to linear-elastic and elasto–plastic response regimes.*

DISTRIBUTION LIST

Elasto–Plastic 3D Finite Element Contact Analysis of a Hole Containing a Circular Insert in a Fatigue Test Coupon

Witold Waldman

AUSTRALIA

DEFENCE ORGANISATION	**No. of Copies**
Task Sponsor	
OIC-ASI-DGTA	1
S&T Program	
Air Force Scientific Adviser	1
Navy Scientific Adviser	1
Chief of Aerospace Division	1
Research Leader, Airframe Technology and Safety Branch	1
Research Leader, Aircraft Structures Branch	1
Research Leader, Aircraft Health and Sustainment Branch	1
Witold Waldman (Author)	1
Ben Dixon	1
Manfred Heller	1
Xiaobo Yu	1
Rebecca Evans	1
Weiping Hu	1
Kevin Walker	1
Chris Wallbrink	1
Michael Opie	1
Andrew Gregory	1
Stephen Sanderson	1
Madeleine Burchill	1
John Wang	1
Loris Molent	1
Jireh Choi	1
DST Group Library	
Library, Edinburgh	1
UNIVERSITIES AND COLLEGES	
Monash University	
Professor Rhys Jones, Department of Mechanical and Aerospace Engineering	1
Professor Wing Kong Chiu, Department of Mechanical and Aerospace Engineering	1
RMIT University	
Professor Chun Wang, School of Aerospace, Mechanical and Manufacturing Engineering	1

Professor Adrian Mouritz, School of Aerospace, Mechanical and Manufacturing Engineering 1

OUTSIDE AUSTRALIA

UNIVERSITIES AND COLLEGES

Mississippi State University

Professor James C. Newman, Jr, Department of Aerospace Engineering 1

Total number of copies: 28

DEFENCE SCIENCE AND TECHNOLOGY GROUP DOCUMENT CONTROL DATA	1. DLM/CAVEAT (OF DOCUMENT)

2. TITLE	3. SECURITY CLASSIFICATION (FOR UNCLASSIFIED REPORTS THAT ARE LIMITED RELEASE USE (L) NEXT TO DOCUMENT CLASSIFICATION)
Elasto–Plastic 3D Finite Element Contact Analysis of a Hole Containing a Circular Insert in a Fatigue Test Coupon	Document (U) Title (U) Abstract (U)
4. AUTHOR(S) Witold Waldman	5. CORPORATE AUTHOR Defence Science and Technology Group 506 Lorimer St Fishermans Bend Victoria 3207 Australia

6a. DST GROUP NUMBER	6b. AR NUMBER	6c. TYPE OF REPORT	7. DOCUMENT DATE
DST-Group-TR-3140	AR-016-369	Technical Report	August 2015

8. FILE NUMBER	9. TASK NUMBER	10. TASK SPONSOR	11. NO. OF PAGES	12. NO. OF REFERENCES
2015/1042651/1	AIR 07/283	OIC-ASI-DGTA	52	17

13. OBJECTIVE ID	14. RELEASE AUTHORITY
AV9430901	Chief, Aerospace Division

15. SECONDARY RELEASE STATEMENT OF THIS DOCUMENT

Approved for public release

OVERSEAS ENQUIRIES OUTSIDE STATED LIMITATIONS SHOULD BE REFERRED THROUGH DOCUMENT EXCHANGE, PO BOX 1500, EDINBURGH, SA 5111

16. DELIBERATE ANNOUNCEMENT

No Limitations

17. CITATION IN OTHER DOCUMENTS

Yes

18. DST GROUP RESEARCH LIBRARY THESAURUS

Holes, Stress concentration, Fatigue life extension, Finite element analysis, Plasticity, Numerical modelling, Numerical simulation, Inserts, Pins, Aircraft structure,

19. ABSTRACT

Aircraft structures typically contain large numbers of circular holes that are fitted with fasteners such as bolts or rivets. During the service life of aircraft, fatigue damage often occurs at such holes. The analysis of the stress distributions occurring around the boundaries of holes in the presence of fasteners is therefore of importance in fatigue life studies, particularly at higher load levels where the effects of material plastic deformation become significant. This report is primarily concerned with the results of a three-dimensional elasto–plastic finite element contact analysis of a typical aluminium fatigue test coupon containing a hole that is fitted with a zero-clearance titanium fastener. The response to separate tension and compression loading was considered. The peak levels of stress concentration and their locations in the presence of varying amounts of material plasticity were determined. The elasto–plastic study was augmented by a 3D linear-elastic investigation of the stress concentration behaviour when the hole is fitted with low-tolerance fasteners that have varying levels of clearance. The linear-elastic and elasto–plastic results presented here are relevant for use in test interpretation and validation activities in relation to the full-scale fatigue test of the BAE Systems Lead-In Fighter Hawk jet trainer aircraft in service with the Royal Australian Air Force.